Subcontractor Report

Nanostructure of a-Si:H and Related Alloys by Small-Angle Scattering of Neutrons and X-Rays

Annual Technical Progress Report
22 May 1999—21 August 2000

Don L. Williamson
Colorado School of Mines
Golden, Colorado

NREL

National Renewable Energy Laboratory

Nanostructure of a-Si:H and Related Alloys by Small-Angle Scattering of Neutrons and X-Rays

Annual Technical Progress Report
22 May 1999—21 August 2000

Don L. Williamson
Colorado School of Mines
Golden, Colorado

National Renewable Energy Laboratory

1. EXECUTIVE SUMMARY

1.1 PREFACE

This report presents results of Phase II research performed from May 22, 1999 to August 21, 2000 under a cost-reimbursable subcontract from the National Renewable Energy Laboratory (NREL, a national laboratory of the U.S. Department of Energy operated by Midwest Research Institute) to the Colorado School of Mines (subcontract number XAK-8-17619-31 to the prime contract DE-AC36-83CH10093). Due to a contract extension and an associated delay in funding, this report covers the above period of more than one calendar year. The research was carried out under the direction of Don L. Williamson, Professor of Physics. Materials characterization, including small-angle x-ray scattering and x-ray diffraction, was carried out in the Physics Department of the Colorado School of Mines (CSM). In addition, small-angle neutron scattering (SANS) was carried out at the NIST Center for Neutron Research. The materials for analyses were supplied by NREL-supported device-making groups as well as by other groups with relevant expertise. The co-P.I., David Marr, of the Chemical Engineering Department of CSM, contributed to the research project via assistance in the design and execution of the SANS experiments at NIST. Graduate students T. Abdel-Monem and D. Charters contributed to the research effort in the x-ray lab at CSM. Various complementary measurements on some of the samples were made at NREL: H. Moutinho - AFM measurements; J. Webb and L. Gedvillas - IR measurements; A. Swartzlander-Guest – EPMA measurements.

1.2 OBJECTIVES/APPROACH

The general objective of this research is to provide detailed microstructural information on the amorphous-silicon-based, thin-film materials under development for improved multijunction solar cells. Correlation of this microstructure with opto-electronic properties and device performance is an integral part of the research. The principal experimental techniques used are small-angle x-ray scattering (SAXS), small-angle neutron scattering (SANS), and conventional x-ray diffraction (XRD). These provide quantitative microstructural data on microvoid fractions, sizes, shapes, preferred orientations, hydrogen clustering, microcrystallinity, and medium-range order. An important task is to establish whether SANS can be used to determine the hydrogen nanostructure and any changes that might occur due to light soaking. Some experiments are conducted using anomalous SAXS (ASAXS) via special facilities in Germany. This method

provides information on the Ge uniformity and nanostructure in a-SiGe:H alloys. Several types of material have been investigated during this second phase of the research in collaboration with the NREL National Team devoted to amorphous silicon solar cell research and development.

1.3 CONCLUSIONS

1.3.1 SANS Experiments

The heterogeneity of a-Si:H and a-Si:D films has been probed on the nano-scale by small-angle neutron scattering (SANS). Films were deposited by two techniques, plasma-enhanced chemical-vapor deposition (PECVD) and hot-wire chemical-vapor deposition (HWCVD) using conditions that yield high-quality films and devices. Four samples were examined in a light-soaked state (AM1, 300 h) and then re-examined after annealing (190°C, 1 h) *in-situ* to look for any change in SANS associated with the Staebler-Wronski effect. No changes were observed in the SANS intensity to a precision that could have readily detected the 25% change reported in 1985 (Chenevas-Paule *et al*). Significant differences are observed in hydrogenated and deuterated films, as well as in the PECVD versus the HWCVD materials. These initial experiments establish that statistically significant SANS data can be obtained from device-quality films so further experiments are planned.

1.3.2 RF-PECVD versus VHF-PECVD Comparison at Higher Deposition Rates

The advantage of using very high frequencies for preparation of a-Si:H materials at high rates (above 5 Å/s) for intrinsic layers (i-layer) of solar cells has been well documented. In an effort to identify film properties which may be related to this superior device performance, a study has been made of the structural, optical and electrical properties of films prepared by ECD at various deposition rates between 1 and 15 Å/s using rf frequencies of 13.56 and 70 MHz. The films were characterized using a number of techniques including small-angle x-ray scattering, infrared absorption spectroscopy, and scanning electron microscopy. For the films made using the 70 MHz frequency, the amount of nanovoids with sizes of < 100Å increases systematically as the deposition rate increases beyond 5 Å/s. Accompanying the increase in void fraction in the films are increases in the hydrogen content and the amount of 2070 cm^{-1} mode in the infrared absorption spectra. In addition to an increase in the amount of nanovoids in the films as the deposition rate exceeds 5 Å/s, the films made using the 13.56 MHz and high deposition rates have larger amounts of SAXS related

to scattering features with sizes > 200 Å. This scattering is associated with large bulk density fluctuations and/or enhanced surface roughness. None of the films in the study displayed signs of having columnar-like microstructures. The nanovoids are not related to changes in the solar cells with increasing i-layer deposition rate for both fabrication processes, perhaps due to the relatively small volume fractions of less than 0.2% and/or good void-surface passivation. However, the larger-scale structures detected in the films made using the 13.56 MHz technique could cause the observed poorer performance in cells prepared at high growth rates.

1.3.3 Ultra-high Deposition Rate HWCVD a-Si:H

SAXS studies of the films grown at NREL in the HWCVD tube reactor reveal a significant increase in the nanovoid volume fraction when converting from one to two filaments to reach the ultra-high deposition rates of up to 1 μm/min. Compared to the one-filament films made near 2 nm/s, all two-filament films have an increase in integrated SAXS of at about two orders-of-magnitude, corresponding to about 1-2 vol.% voids. This increased SAXS is independent of deposition rate (with two filaments) from about 3 to 13 nm/s. Similarly, x-ray diffraction studies of the medium-range-order show no variation in order over this same rate change. The order is not as good as detected in the best quality PECVD and HWCVD films reported earlier.

1.3.4 "On-the-Edge" a-Si:H

Early Crystallization Study

PECVD films prepared by USSC under different H dilution conditions have been examined by IR, XRD, and H evolution. The high-H-dilution material is deemed "on-the-edge" material because of its observed tendency to be near the boundary between amorphous and microcrystalline states. Upon annealing, a low temperature H-evolution peak appears, and film crystallization is observed at temperatures as low as 500°C, which is far below that observed for a-Si:H films grown without H dilution. Although not detected directly by XRD in the as-grown state, very small crystallites are postulated that catalyze the low-temperature crystallization of the films upon annealing. The large spatial inhomogeneity in the H bonding associated with the very small crystallites is suggested to be one of the reasons for the reduced Staebler-Wronski effect observed in solar cells utilizing the "on-the-edge" material.

Electronic States/XRD Study

Thin film n-i-p solar cells were prepared by USSC using decomposition of disilane-hydrogen mixtures by plasma-enhanced chemical vapor deposition. By increasing either the H dilution ratio or the thickness, the i-layer structure showed a transition from amorphous to microcrystalline silicon characterized by x-ray diffraction at CSM. The electronic states of the i-layer were examined by photoluminescence (PL) spectroscopy at UNC, which showed that: (a) below the onset of microcrystallinity, a blueshift of the 1.4 eV PL peak energy along with a decrease of the band width occur as the structural order is improved; (b) above the onset of microcrystallinity, the PL efficiency decreases by a factor of 4-5 and the PL peak energy is redshifted toward 1.2 eV as the μc-Si volume fraction is increased. In addition, the solar cell open circuit voltage shows first an increase and then a decrease, correlating with the PL peak energy position. We conclude that the PL spectroscopy is a sensitive tool for characterizing the gradual amorphous-to-microcrystalline structural transition in thin film solar cells.

1.3.5 ASAXS Experiments and Analyses

From extended anomalous-SAXS (ASAXS) measurements at numerous x-ray energies, structural and physical properties such as non-uniform Ge-concentrations and – in combination with flotation density results – the densities of Ge-enriched regions in amorphous a-$Si_{1-x}Ge_x$:H alloys were deduced based on a two-phase model. Depending on the preparation technique (with and without H dilution of the source gases), a dense phase with volume fractions of about 90% and with Ge-enrichments only slightly higher with respect to the entire alloy were observed. These denser regions with average sizes between 10 and 23 nm can be interpreted as a phase containing slightly enhanced numbers of homopolar Ge-bonds, surrounded by a small volume fraction phase of low density, H-rich regions containing much less Ge (sometimes none) with averages sizes from 0.6 to 1.6 nm.

1.3.6 BP-Solarex SAXS/MRO Study

BP-Solarex supplied films of their latest device-quality a-$Si_{1-x}Ge_x$:H materials (x= 0 to 0.44) for study by SAXS and XRD. The SAXS shows nanostructures typical of such alloys, increasing strongly with Ge additions. The x=0 material has a somewhat larger volume fraction (0.05%) of

nanostructural features than the best PECVD materials prepared by USSC (0.01%). The medium-range order (MRO) shows a slight decrease with added Ge and all the films show reduced order compared to the best-quality PECVD and HWCVD films prepared by other groups.

1.3.7 High-Pressure Study

At the request of the UCLA group, two SAXS samples were supplied for a high pressure experiment: NREL-HWCVD a-Si:H films on 10 micron Al foil, folded into 8 layers;

T840 - low substrate temperature, relatively high void fraction (about 2 vol.%)

T905 - high substrate temperature, very low void fraction (about 0.02 vol.%)

A SAXS-reference Al-substrate foil was included in the high pressure treatment of the above samples. Careful SAXS measurements after the high-pressure treatment at 3 kbar show that there is no evidence for a residual microvoid collapse.

1.3.8 "Polymorphous" Si:H

We have completed SAXS measurements from a series of a-Si:H samples that are designated as "polymorphous" to describe a new type of a-Si:H prepared by P. Cabarrocas of the Ecole Polytechnique. The SAXS due to any nanostructural features (< 10 nm) is extremely weak. Three samples show an integrated SAXS only slightly larger than the detection limit corresponding to 0.01 vol.% voids. Thus, it is very interesting that there is little or no scattering from the "polymorphous" nature of these films. This may be due to a very small electron density contrast between the incorporated nanocrystals that are seen by TEM and the amorphous matrix, and/or due to a very small volume fraction of such nanocrystals (however, Cabarrocas has pointed out that he expects the films to have large volume fractions). XRD on all the polymorphous samples did not detect any evidence of crystalline Si (111), (220), or (311) peaks.

1.3.9 Microcrystalline Si:H

Due to increased interest in microcrystalline Si for possible solar cell applications, three sets of such material from different groups were examined by SAXS.

<u>HMI Material</u>

SAXS and density measurements have been completed on four μc-Si:H samples sent by M. Birkholz of the Hahn-Meitner-Institut (HMI). The SAXS signals are quite strong and there are not

dramatic differences in the 4 samples prepared at different substrate biases. The average diameters of the scattering objects were 4 to 6 nm. The integrated intensity from the nanostructural features was used to estimate a volume fraction of voids in the range of 7 to 11 vol.%, assuming this is the origin of the SAXS. [The interpretation of the SAXS from microcrystalline material is complex - is it due to voids within the microcrystalline matrix, or is is due to the microcrystals themselves surrounded by a low-density residual amorphous phase?] The effect of tilting 2 of the samples is consistent with elongated scattering objects oriented with their long axis along the growth direction. Thus the above sizes represent the size of the small dimension of elliptical objects. We measured the x-ray diffraction patterns from the samples and observed linewidths corresponding to crystallites 12 to 30 nm in size.

ECD Gas Jet Material

Four samples of μc-Si:H prepared by the gas-jet technique developed at ECD were examined by SAXS. The silane flow was increased from 15 to 45 sccm for the series of samples and the integrated SAXS was found to decrease systematically from a high value corresponding to about 11% voids to a value for about 1.5% voids. This is consistent with an expected trend of decreasing amount of microcrystalline material with increasing gas flow. This was confirmed by XRD. The scattering features are only about 2 nm in diameter and show a relatively weak tilting effect.

IPE Material

Four films of μc-Si:H prepared by the HWCVD method at the Institute of Physical Electronics (IPE) of the University of Stuttgart have been examined by SAXS. This series was made as a function of deposition pressure and yielded a minimum in the integrated SAXS at the intermediate value of 40 mTorr. The corresponding void volume fractions range from 11 to 6 %, again very high and apparently typical of microcrystalline material. The sizes of the scattering features range from 6 to 9 nm and clear, but relatively weak, tilting effects are observed.

Table of Contents

List of Figures

List of Tables

2. INTRODUCTION

Several experiments have been completed during Phase II of this research project in collaboration with NREL and NREL-supported groups, as well as with other groups having expertise in the field of amorphous and microcrystalline silicon-based solar-cell materials. The first SANS experiments have been performed at the NIST Center for Neutron Research in Gaithersburg, Maryland during three days of beam time awarded to us in August 1999. First results were reported at the NCPV Program Review meeting and the MRS meeting, both in April 2000. The first section below summarizes these results and documents the good quality SANS data from device-quality films. The results and discussion of the in-house SAXS and XRD experiments are divided into sections describing our experiments in collaboration with NREL, ECD, USSC, UNC, BP-Solarex, UCLA, Ecole Polytechnique (France), DESY (Germany), HMI (Germany), and IPE (Germany) addressing nanostructural issues with a variety of materials and deposition methods.

3. RESULTS AND DISCUSSION

3.1 SANS Experiments

It has long been clear that hydrogenated amorphous silicon (a-Si:H) and related alloys such as a-SiGe:H and a-SiC:H are heterogeneous on the micrometer and nanometer length scales. This information has come from many techniques including electron microscopies, x-ray and neutron diffraction and scattering, scanning-probe microscopies, and nuclear magnetic resonance. The degree of heterogeneity depends strongly on the deposition methods and detailed conditions, and generally one is striving to eliminate, minimize, or control any non-uniformity in the quest for the optimum material for a given application. Our work has focused mainly on x-ray methods in the recent past to study a wide range of a-Si:H-based materials, with particular emphasis on solar-cell-quality material. These studies utilize small-angle x-ray scattering (SAXS) to look for electron density fluctuations [1,2] and x-ray diffraction (XRD) to examine medium-range order and microcrystallinity [3,4]. Due to the controlling influence of hydrogen in this class of materials, techniques which provide special sensitivity to the hydrogen are particularly valuable. Due to the much larger relative cross-section for scattering of neutrons vis-à-vis x-rays from hydrogen atoms, small-angle neutron scattering (SANS) should be much more sensitive to the hydrogen distribution than SAXS. However, only a few experimental SANS studies of a-Si:H have been reported [5-10], primarily due to needs for rather thick samples and special facilities. Also, weak to non-detectable

signals were reported for the best quality films [5]. Recent demonstrations of good quality SANS data from very thin polymer films using signal-to-noise-enhancing conditions at the NIST Center for Neutron Research (NCNR) [11,12] encouraged us to attempt new experiments with high-quality a-Si:H. The possibility of separating out the signals due specifically to the hydrogen heterogeneity (from that due, e.g., to microvoids or surface roughness) and reducing the inherently strong incoherent background scattering due to hydrogen is allowed by substituting deuterium for hydrogen [8,13,14], so we have included such samples in our first experiments as well.

Of particular interest from previous SANS work was the report of an intriguing experiment related to the Staebler-Wronski effect [9]. Using reactively-sputtered a-Si:H, grown 20 μm thick on a fused silica substrate at 300°C, the material was first checked to show a 30% increase in ESR spin density between the annealed (180°C) and illuminated states (4 h of visible light). No other opto-electronic or structural data were provided for this one sample investigated. The SANS was then measured in this light-soaked condition (state B), followed by an anneal to return to state A, and the SANS re-measured. A 25% drop in intensity was observed, with no apparent change in the angle dependence. The illumination was then repeated and a 25% increase in intensity was seen. In order to explain this rather dramatic, reversible change in the SANS at all angles, a relatively long-range (~10 nm) reversible motion of H between the two states is required as suggested by applying a model developed earlier [15] to indicate the movement of H to (during illumination) and from (during annealing) the low density boundary regions surrounding the dense matrix regions [16]. Our experiments were designed to include a search for such a light-induced effect.

SANS Experimental Details

Two types of a-Si:H films were prepared for the SANS studies: PECVD and HWCVD material grown under conditions similar to those that yield high efficiency solar cells [17,18]. A comparison of these two materials is of current interest due to evidence of differences in structural features, particularly in the hydrogen distributions [4]. To optimize signal-to-noise [11,12], special c-Si substrates were used with the following specifications: float-zone wafers, 500 μm-thick (± 25 μm), undoped (resistivity>1000 Ω-cm), two-side polished with low surface roughness (<0.5 nm rms roughness, confirmed by AFM to be about 0.15 nm), (100) orientation. The wafers were diced into 2.5 cm x 2.5 cm squares to allow films to be grown with at least a 2.4-cm-diameter area to take advantage of the maximum neutron beam diameter available (2.2 cm). To minimize adhesion

problems and allow bulk light-soaking, films were grown to thicknesses of 1 to 2 μm. Multiple films were grown under nominally identical conditions to allow stacking of up to 20 layers. The neutron absorption by the c-Si substrates at a thickness of 1 cm (20 substrates) is only about 3 %.

PECVD films were grown with either $SiH_4 + H_2$ or $SiD_4 + D_2$ and HWCVD films with SiH_4 or SiD_4. PECVD samples were grown with "high dilution" of $H_2(D_2)$, which yields the best devices [17] and improved medium-range order [3]. HWCVD samples were grown at elevated substrate temperatures (360^oC) which yields lower saturated defect densities, better devices [18], and improved medium range order [4] compared to lower substrate temperatures. One slight modification from typical HWCVD conditions was to use two filaments in order to produce films of uniform thickness over an area that allowed simultaneous deposition on 4 of the substrates. As will be discussed, this modification apparently led to enhanced heterogeneity. Prior to the SANS measurements the four sets of films were subjected to 300 h light soaking under AM1.5 conditions.

The SANS measurements were made on the 30 m beam-line NG-3 of the NCNR [19]. Data were collected in an area detector (64 cm x 64 cm, 1 cm resolution) over a momentum transfer range from q = 0.05 nm^{-1} to 3 nm^{-1} [q = $(4\pi/\lambda)sin\theta$, where 2θ is the scattering angle and λ is the neutron wavelength] using two detector positions (2 m and 13 m from the sample). A wavelength of 0.6 nm was selected with a spread of $\Delta\lambda/\lambda = 34\%$, which prevented any double-Bragg diffraction from the c-Si substrates and allowed a neutron flux at the sample of the order of 10^6 $cm^{-2}s^{-1}$. The samples were mounted in a chamber that allowed multiple (up to 7) sample mounting, a vacuum to reduce background scattering, and *in-situ* sample annealing. The four samples which had been previously light-soaked were measured in this state (Staebler-Wronski state B), then annealed *in-situ* at 190^oC for 1 h (Staebler-Wronski state A), then remeasured without disturbing except to shift from one sample to the other via the automatic sample changer. The observed two-dimensional SANS intensities were apparently circularly symmetric for all samples and therefore circularly averaged and converted to absolute cross-section values, $d\Sigma/d\Omega$ ($cm^{-1}ster^{-1}$), using standard procedures [19] that included subtracting the incoherent scattering (q-independent) from the substrates. The latter was measured with a stack of c-Si substrates of the same thickness as the stack for a given sample (either 12 or 19 layers for the present samples) and confirmed to be q-independent and of the correct magnitude ($1.2x10^{-4}$ $cm^{-1}ster^{-1}$) thereby demonstrating that no extra scattering was coming from our carefully selected substrates.

Results and Discussion of SANS Experiments

Figure 1a compares the SANS data obtained from the a-Si:H and a-Si:D films prepared by PECVD under high H_2 or D_2 dilution conditions, respectively. These data are from the samples in the light-soaked state B. There is no obvious change in the SANS after annealing, state A (data not shown), and the ratios of intensities obtained from these two states for both samples are displayed as the lines near unity in Fig.1. There are several features of interest: (i) the presence of SANS intensities well above the noise for device-quality material; (ii) the large difference in the intensities; (iii) the clear leveling off at a constant intensity for the a-Si:H film. Suspicious of the dramatic difference in the SANS between the a-Si:H and a-Si:D, both samples were checked by x-ray diffraction and a small but clear signal from microcrystalline Si was detected in the a-Si:D sample superimposed on the dominant a-Si:D diffraction typical of the amorphous phase [4], while the a-Si:H sample was fully amorphous. This was checked in several of the duplicate layers prepared in separate deposition runs. Thus, we attribute the enhanced SANS in the "a-Si:D" sample to added heterogeneity associated with D-free microcrystals surrounded by D-rich regions. Although the deposition conditions were nominally the same for the hydrogenated and deuterated films, it is now established that the high-hydrogen-dilution condition is operating near the onset of microcrystal formation and improved medium-range order [3,4]. Somehow the substitution of deuterium has modified this onset condition, at least for the c-Si substrates. The constant intensity of about 0.04-0.05 $cm^{-1}ster^{-1}$ for the a-Si:H film is in close agreement with the expected incoherent scattering from an alloy with 12 at.% H, which was found from IR absorption measurements on this sample. The SANS at high q for the deuterated sample drops below that of the hydrogenated sample, consistent with the lower incoherent cross-section for D versus H, but the drop is not as much as expected assuming a similar D content of 12 at.%.

Figure 1b shows SANS data from a-Si:H and a-Si:D prepared by HWCVD at elevated (360°C) substrate temperature. In addition to state B/state A intensity ratios near unity, other noteworthy features include: (i) a much stronger intensity and different q-dependence than the PECVD a-Si:H; (ii) a drop to lower intensity than the PECVD a-Si:H at the highest q; (iii) only
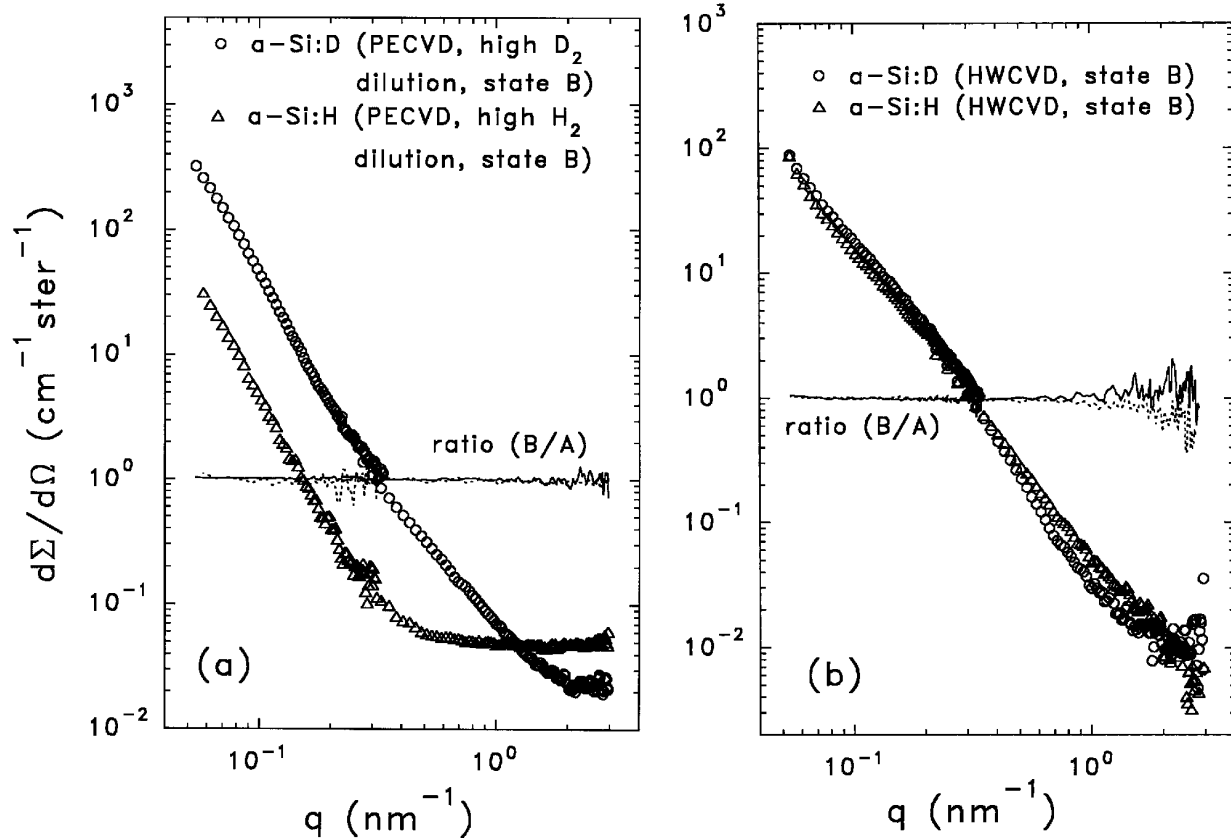
Fig. 1. SANS data from (a) PECVD films and (b) HWCVD films grown on c-Si substrates. Ratios of the light-soaked (state B) SANS intensities to the annealed (state A) intensities are shown as the solid (a-Si:D) and dashed (a-Si:H) lines.

slight differences in the intensities from the hydrogenated and deuterated films. The enhanced SANS compared to the PECVD a-Si:H is definitely not related to microcrystallinity as confirmed by x-ray diffraction. Previous SAXS studies showed the best quality HWCVD material to contain a maximum void fraction of 0.01 vol.% [1]. Analysis of the SANS data is underway using similar approaches [1], but fractions well above this level are indicated. Recent studies of ultra-high-deposition rate material [20] included the use of a second filament, similar to the geometry used to produce the SANS sample studied here, and it has been found that the SAXS intensities are much higher than those with a single filament at the same deposition rate of about 2 nm/s used for the SANS samples. The photo-sensistivity of this two-filament material is extremely good [20], in spite of the strong SAXS indicative of 1 to 2 vol.% voids. This issue is under further investigation. The lower intensity at high q is consistent with a lower H content, determined to be about 3 at.% in the a-Si:H film by IR.

In order to compare the SANS intensities in the states A and B, ratios of the data (as displayed in Fig.1), were computed with appropriate weighting by the statistical error at each q. Results from all four samples studied are listed in Table I by averaging the data sets for the two detector positions (q = 0.05 to 0.34 nm^{-1}, q = 0.22 to 3.0 nm^{-1}). These values can be compared with the previous ratio of about 1.25 over the q range from 0.04 to 0.25 nm^{-1} [8]. It is difficult to speculate on the origin of the discrepancies in these results due to lack of experimental details provided in the previous experiment. Possible issues involve the degree of light degradation that would occur with only a 4-h light soak of a 20-μm-thick film and whether the sample needed to be removed from the beam line for the annealing and light soaking treatments. The latter would require careful replacement in exactly the same geometry to avoid changes in intensity, particularly if the material had a columnar-like structure which causes a high sensitivity of the sample orientation to the beam [1,5].

We have examined the degree of light-induced degradation of companion samples to those shown in Table I. Solar cells with i-layers made under the same conditions as the two PECVD samples in Table I showed degradation of the fill-factor after 412 h of light soaking of 6.9% and 3.1% for a-Si:H and a-Si:D, respectively, with a recovery within 0.8% of both initial values after an anneal at 175°C for 1 h. The photoconductivity of the HWCVD companions was monitored over 600 h of light soaking, the a-Si:D degrading from 2.4x10^{-4} to 2.7x10^{-5} Ω^{-1}cm^{-1}, a factor of 9, and the a-Si:H degrading from 4.2x10^{-5} to 1.0x10^{-5} Ω^{-1}cm^{-1}, with both recovering to slightly higher than the initial values after annealing at 190°C for 1 h. These results confirm that significant Staebler-Wronski effects were induced in the SANS films investigated.

Table I. Ratio of SANS intensities in state B (light-soaked) versus state A (annealed).

Sample	SANS intensity ratio (B/A) (q = 0.05 to 0.34 nm^{-1})	SANS intensity ratio (B/A) (q = 0.22 to 3.0 nm^{-1})
a-Si:H, PECVD, high dilution	0.96 ± 0.08	0.97 ± 0.07
a-Si:D, PECVD, high dilution	1.02 ± 0.03	1.00 ± 0.04
a-Si:H, HWCVD, 360°C	1.00 ± 0.04	0.93 ± 0.07
a-Si:D, HWCVD, 360°C	0.99 ± 0.03	1.00 ± 0.08

Conclusions from SANS Experiments

The previous Staebler-Wronski-effect-induced change in nanostructure observed by SANS experiments several years ago [9] could not be reproduced in the present study. No detectable changes were found to a precision as good as ± 3%. This is consistent with the very small structural changes being observed in association with the Staebler-Wronski effect [21]. We also established that statistically-significant SANS data can be obtained from device-quality films. The signals are well above the incoherent scattering from the H so it is not crucial to replace H with D, although such isotope substitution experiments should, in principle, allow separation of hydrogen-related nanostructure from other scattering features. However, the present observed differences in hydrogenated versus deuterated PECVD material are due in part to actual changes in the deposition process in the "high-dilution" regime such that a transition to partially microcrystalline material occurs with the deuterated gases. Also, the use of two filaments versus one in the HWCVD process is somehow inducing enhanced heterogeneity. Further analysis of the SANS intensities versus q is underway based on various models of the hydrogen and void nanostructure as well as possible surface roughness effects, supported by AFM studies.

3.2 RF-PECVD versus VHF-PECVD Comparison at Higher Deposition Rates

The advantage of using very high frequencies (70-100 MHz) to prepare i-layers for a-Si:H solar cells at deposition rates between 5 and 10 Å/s has been reported by several research groups [22-25]. As the deposition rate for the a-Si:H i-layer growth is increased from 1 to 10 Å/s, virtually no change is observed in the solar cell properties, such as the fill factor (FF), the open circuit voltage (V_{oc}) and the short circuit current (J_{sc}). Only a 5% drop in J_{sc} is noted for a-Si:H cell with the same thickness prepared with current-enhancing Ag/ZnO backreflectors. In contrast, extensive attempts to increase the i-layer deposition rates using the standard 13.56 MHz PECVD process has led to cells with poor fill factors and cell efficiencies. This poorer performance is usually attributed to enhanced powder and polyhydride formation in the plasma that leads to i-layers with defect ridden, heterogeneous microstructures.

Here, optical and structural properties for single-layer films prepared at a variety of deposition rates using either a 13.56 or a 70 MHz frequency are compared with the performance of nip solar cells whose intrinsic layers were prepared under identical conditions to those for the single-layer films. The measurements include small-angle x-ray scattering (SAXS), infrared absorption

spectroscopy (IR), optical absorption spectroscopy and scanning electron microscopy (SEM). With these comparisons, a determination of which film properties play a role in determining the device performance can be made.

Experimental Details

The a-Si:H films and nip solar cells were fabricated using a research-scale, multi-chamber, load-locked deposition system. The system has three separate chambers for deposition of n-type, p-type and intrinsic layers. For preparation of the single-junction solar cells, stainless steel substrates without current-enhancing Ag/ZnO backreflectors were used for preparation of the semiconductor structures. The thin doped layers were prepared using the conventional PECVD process in which a 13.56 MHz RF signal is used. To fabricate the a-Si:H i-layers, either the standard 13.56 MHz frequency or a fixed VHF frequency of 70 MHz was used. In this study of the general effects of deposition rate on film and device performance, a large set of parameters was altered to look for systematic trends with deposition rate. After fabrication of the nip structure, the devices were completed by evaporative deposition of indium tin oxide (ITO) conductive layers and then aluminum (Al) collection grids.

To characterize the cells, current vs. voltage (IV) and spectral response (quantum efficiency) measurements were made. For the IV measurements, white AM1.5 light was used to obtain the IV data. For light soaking studies, the cells were subjected to 600 h. of one Sun light with the cell temperature fixed at 50ºC. The i-layer thicknesses were determined using capacitance techniques.

For the SAXS [1] and SIMS measurements, 1 μm a-Si:H films were deposited on 10-μm-thick, 99.999% Al substrates with both types of measurements performed with the same samples. IR and SEM measurements were made using 1 μm a-Si:H films deposited on crystalline Si substrates while 1 μm a-Si:H films on 7059 glass were used for optical absorption analysis.

Results

To study the heterogeneity of the films as the deposition rate was varied, films were prepared under a variety of conditions for SAXS analysis using both plasma frequencies. It was found that for films made using either the RF (13.56 MHz) or VHF (70 MHz) methods, the amount of SAXS increased as larger deposition rates were used. Figures 2 and 3 compare SAXS data for films prepared at 1-3 and 9-10 Å/s for a-Si:H films made using the 70 and 13.56 MHz frequencies.

While the total amount of scattering increased for the films using both frequencies, detailed analysis of the SAXS data demonstrated that there are differences in the microstructural changes between the films made using the two different techniques. Through this analysis, the SAXS from a-Si:H films can be attributed to three different sources [1] ; 1) nanovoids with sizes less than 100Å, 2) larger scale structures having sizes greater than 200Å, and 3) diffuse scattering due to atomic-scale density fluctuations.   For both deposition techniques, the volume fraction of nanovoids increases as the deposition rate goes beyond 5 Å/s as is shown in Fig. 4 where the integrated SAXS related to the nanovoid fraction (Q_n) [1] is plotted as a function of deposition rate. As can be seen from the data in the figure, at the higher deposition rates (6-10 Å/s), the samples made using the RF method typically have a larger percentage of nanovoids.   In terms of larger-scale structures, the amount of related SAXS is also larger for the films prepared by the lower frequency technique. The Porod slope, calculated from the SAXS data in the small q range [1], is
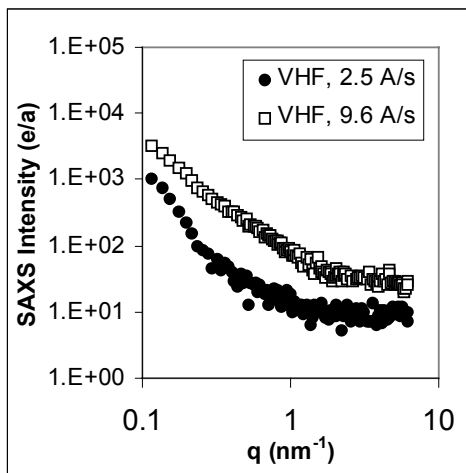

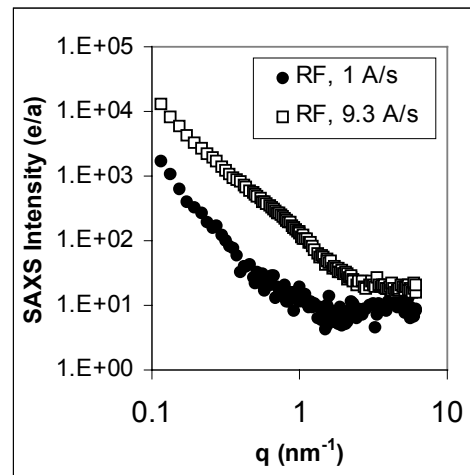Fig. 2. SAXS for VHF prepared films.

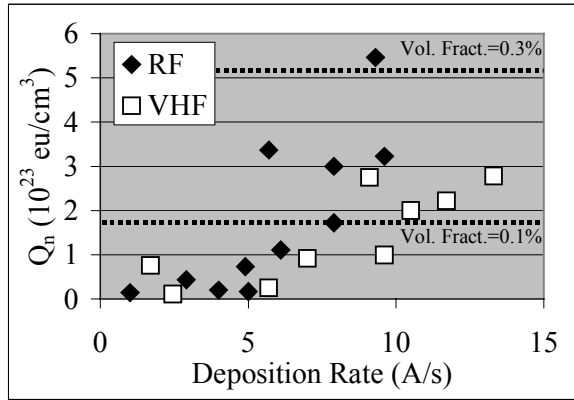

Fig. 3. SAXS for RF prepared films.

Fig. 4. SAXS signal (nanovoids) versus rate.
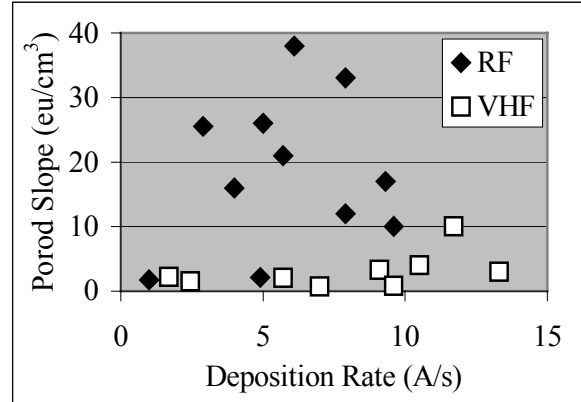

Fig 5. Porod slope versus deposition rate.

related to the scattering from larger-scale heterogeneity (sizes >200 Å) such as density fluctuations from non-uniform hydrogen distributions or from a significant amount of surface roughness.   Fig. 5 shows that the Porod slopes for the films made using the 13.56 MHz and deposition rates above the standard 1 Å/s are typically much higher than those for the 70MHz produced films which remain low independent of deposition rate in the range studied.   Thus, the RF films made at the higher rates have enhanced larger-scale internal heterogeneity and/or rougher surfaces. Preliminary atomic force microscope (AFM) analysis of films deposited at a 10 Å/s rate demonstrate that the film surfaces are rougher when using the RF technique instead of the VHF method.   However, more analysis of this data is needed in order to prove that the larger Porod slopes are entirely due to enhanced surface roughness.   For both the RF and VHF-produced films, the diffuse scattering generally increases with increasing deposition rate consistent with an increase in H content [1] and supported by some IR results presented below.

By measuring the SAXS at different tilt angles, one can determine if the scattering centers which cause the SAXS are highly oriented relative to the film surface as they are for films which have columnar-like microstructures [1]. For all of the films measured in this study, relatively small changes in the SAXS were noted as the samples were measured at different tilt angles. This is demonstrated in Figs. 6 and 7 where SAXS data measured at 0 and 35° tilt angles are compared for a film prepared with the 70 MHz technique at a deposition rate of 10 Å/s (Fig. 6) and a film prepared with the 13.56 MHz method at a 7 Å/s rate (Fig. 7).   Only the data at small q for the sample prepared with the 13.56 MHz frequency decreases slightly with varying angle. The lack of a substantial tilt dependence suggests that all of the films have little in the way of a columnar-like

10

microstructure and that the scattering features detected by SAXS is spherical in nature and/or randomly oriented. The lack of columnar-like structures in the films was confirmed by SEM analysis of the cross-sections of 1 μm-thick films prepared by both techniques at 8-12 Å/s rates. Fig. 8 displays a representative SEM photograph taken at 60,000x of such a 1 μm-thick film demonstrating the lack of any discernable microstructure.
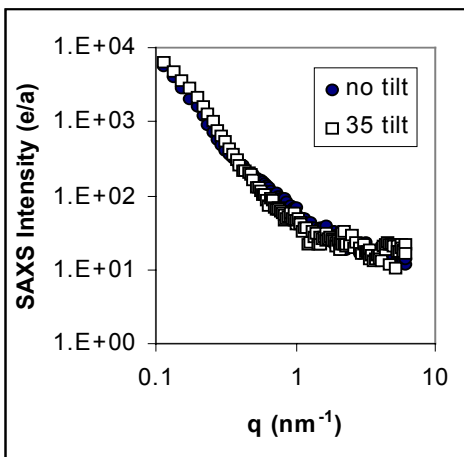

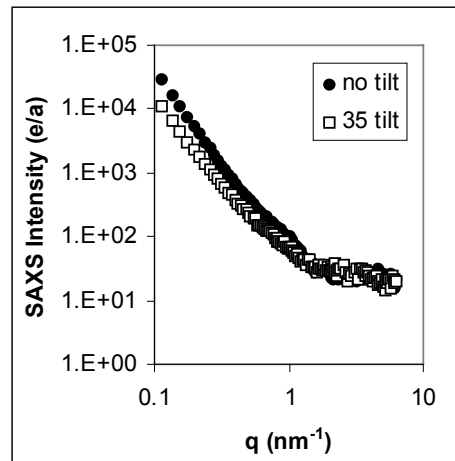Fig. 6. SAXS data for a film prepared by the VHF method at a 10 Å/s rate.

Fig. 7. SAXS data for film prepared by the RF method at a 7 Å/s rate.

Table II compares the SAXS data with data from IR, SIMS and optical absorption measurements of films made at similar deposition conditions. As the amount of SAXS detected nanovoids (Q_n) increases with increasing deposition rate for films made using the VHF technique, the hydrogen content determined by IR measurements increases as does the microstructure factor $R = (2070 \text{ cm}^{-1})/(1970 \text{ cm}^{-1} + 2070 \text{ cm}^{-1})$ determined by the integrated areas under the 1970 cm^{-1} and 2070 cm^{-1} IR peaks. With the increase in hydrogen content, the bandgap also increases. In contrast to these systematic trends for the films produced by the VHF technique, no correlation between the SAXS data and the hydrogen content or the microstructure factor could be made for the samples prepared using the RF method. Besides the trends for the SAXS data, the only systematic observation in the material properties for the films made using the RF technique was an increase in bandgap energy as the deposition rate increased beyond the 5-6 Å/s range.

For comparison of the film properties with device performance, Table III lists properties for a-Si:H nip cells whose i-layers were made using conditions identical to those used to prepared certain

SAXS samples. All of the cells were made without current-enhancing backreflectors and have i-layer thickness of 1500±150 Å. While several measurements suggest that there are structural differences (nanovoids, microstructure factors, and hydrogen contents) for the films made by the VHF technique using the low (1-3 Å/s) and high (8-10 Å/s) rates, little variations are observed for the cell properties. The FF and the amount of cell degradation with light soaking were found to remain constant in this range of deposition rate while only a drop in the J_{sc} value
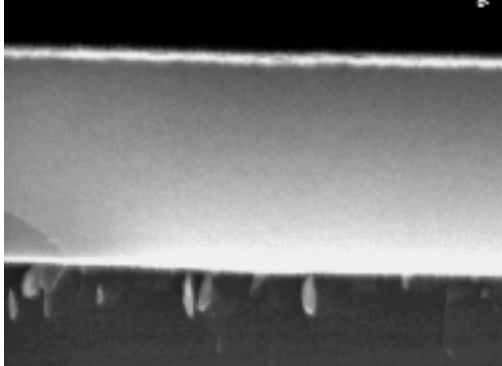

Fig. 8. SEM photograph of the cross section of a RF film made at a 9 Å/s rate.

Table II
Data from SAXS, IR, and optical absorption measurements for films prepared by VHF method.

Dep. Rate (Å/s)	Q_n (10^{23} eu/cm^3)	Vol. Fract. (%)	C_H from IR (at. %)	Microstr. Factor R	E_{gap} (eV)
2.1	0.11	0.01	9.3	0.14	1.76
6.1	0.92	0.05	13.9	0.16	1.79
10.0	2.00	0.12	16.4	0.22	1.86
10.9	2.54	0.15	-	-	1.83

from 9.5 to 8.9 mA/cm^2 lead to a drop in the cell efficiency. An alternative set of deposition conditions lead to the achievement of the 9.6 mA/cm^2 value and a high efficiency without a large change in the Q_n value or the bandgap energy (see the data in Table II for the for the films made at rates of 10 and 10.9 Å/s). In contrast, lower FF values and large amounts of degradation with light soaking are found for the films prepared using the RF method and deposition rates of 5 Å/s or higher. Also, the J_{sc} values are lower at the highest rates, likely due to the same reason that under certain deposition conditions the VHF films prepared at the 10 Å/s also have low currents.

From careful measurements of the high wavelength region of the quantum efficiency spectra, one is able to calculate Urbach energies (E_0) for the i-layer materials using the single-junction cells. In contrast to the J_{sc}, FF and P_{max}, values listed in the table, the E_0 values were obtained after light soaking of the cells. As can be seen from the data listed in the table, no systematic change in E_0 was observed with increasing deposition rate demonstrating that the changes in cell properties are not related to variations in the conduction band tail.

Table III. Properties for a-Si:H cells made using RF and VHF methods.

Freq (MHz)	Deposition Rate (Å/s)	J_{sc} (mA/cm^2)	FF	P_{max} (mW/cm^2)	% of Degradation with Light Soaking	Urbach Energy E_o (meV)
70	2.1	9.38	0.728	6.46	-	-
70	6.1	9.51	0.726	6.45	13.4	47
70	10	8.87	0.732	6.25	15.4	50
70	10.9	9.63	0.733	6.63	12.1	44
13.56	0.9	9.52	0.732	6.47	12.5	48
13.56	5	9.57	0.690	5.98	20.2	46
13.56	5	9.52	0.674	5.88	23.5	47
13.56	8.1	8.95	0.671	5.43	23.8	59
13.56	8.6	8.27	0.684	5.31	18.8	49
13.56	9.2	8.68	0.680	5.47	19.7	48

Discussion and Conclusions

In terms of the effect of the structural properties on the device performance, it is surprising that some of the structural changes noted by the film measurements do not seem to affect the solar cell performance. For the materials made using the VHF technique, all of the structural measurements suggest that as the deposition rate increases, a larger number of randomly oriented nanovoids appear in the films. It seems likely that the surfaces of the nanovoids are coated with hydrogen, leading to the observed increase in the 2070 cm^{-1} mode in the IR spectra as the deposition rate increases. Also, it is clear that this increase in void fraction in the films does not correlate with a change in device performance. It is possible that the change in void fraction is just too small (only about 0.1 vol.%) to have a bearing on the i-layer transport properties.   Also because the IR results suggest that the void surfaces are likely hydrogen coated, the appearance of the additional voids with increasing deposition rate may not lead to an increase in defect density in the i-layers, which may ultimately prove as the determining factor of the cell properties. Measurements of the defect densities for these materials are presently being made.

For the films made using the RF method, no change in the nanovoid fraction is observed when the deposition rate is changed from 1 to 5 Å/s while in this same range of deposition rate a large

change in the cell properties is noted (Table III). Since the SAXS films and the i-layers for the cells were made using nominally the same deposition parameters, this would suggest that, at least for these studies, the nanovoid fraction (well below 0.1 vol.% up to 5 Å/s) does not play a significant role in the determination of the cell properties. However, the larger scale structure (>200 Å) could affect the device performance. While there is not a one-to-one correlation with the Porod slope and the device efficiency, all of the i-layers for cells with FF below 0.7 were prepared under conditions which lead to high Porod slopes (>10 eu/nm^3, Fig. 4). Only the cells prepared using the VHF technique and the cell made using the RF method and a rate near 1 Å/s have FF near 0.73 and each of these conditions lead to low Porod slopes. As mentioned previously, these large scatterers could be related to non-uniform hydrogen distributions and/or to surface roughness. While they do not conclusively prove the nature of the larger scatterers, preliminary AFM measurements do suggest that the surfaces for the RF films made at high rates are rougher. Further measurements are planned to confirm the origin of the large-scale scattering.

3.3 Ultra-High Deposition Rate HWCVD a-Si:H

NREL has developed modifications of a HWCVD processing system to allow extremely high deposition rates of up to 1 μm/min (17 nm/s) [26]. This material maintains a photoconductivity-to-dark-conductivity ratio of 10^5 up to 13 nm/s. Several samples have been prepared by NREL for SAXS and XRD studies. Figure 9 summarizes the integrated SAXS intensities (Q) for a series made with deposition rates up to 13 nm/s in the "L" system. Also shown is a result from a sample made in the "T" system at 1.5 nm/s. Predicted signals due to various void volume fractions are also indicated. Note the sharp increase in SAXS between 1.5 and 3 nm/s. This dramatic change is somehow associated with a change from the use of 1 or 2 filaments. The solid symbols indicate the use of 2 filaments and the open symbols indicate the use of 1 filament. Further samples to investigate higher deposition rates with 1 filament are planned. Note that the data in Fig. 4 for the ECD samples all fall into the range below Q=6x10^{23} eu/cm^3 at the far left (below 1.5 nm/s) in Fig. 9. The x-ray linewidth W of the first scattering peak is shown in Fig. 10 versus deposition rate and is remarkably constant. This indicates little change in MRO between 1.5 and 14 nm/s. The W values are somewhat higher than the narrowest values reported earlier [4] and indicated by the dashed line in Fig. 10, suggesting some deterioration in MRO compared to the best quality PECVD and HWCVD films.
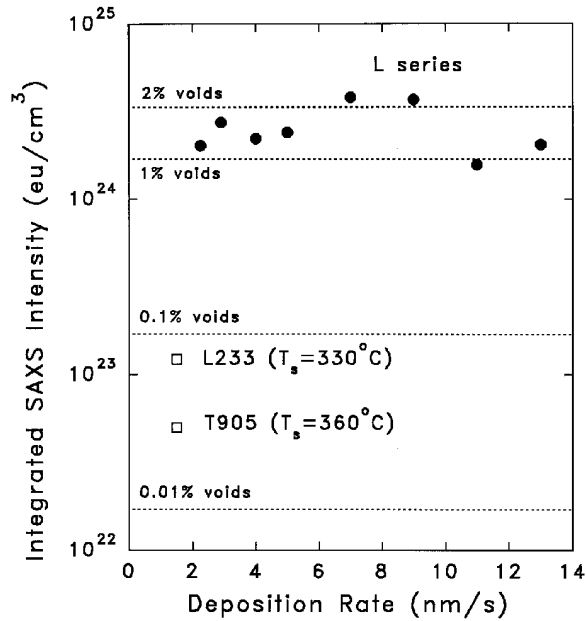
Fig. 9. Integrated SAXS intensities from ultra-high deposition rate HWCVD a-Si:H. Solid (open)symbols – 2 (1) filaments.
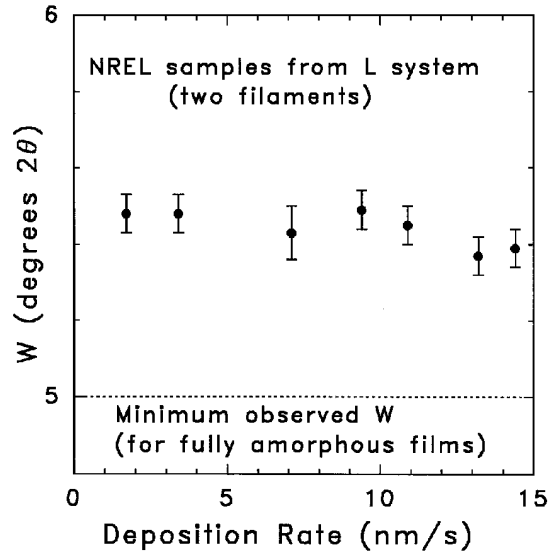
Fig. 10. XRD linewidth from ultra-high deposition rate HWCVD a-Si:H All films made with 2 filaments.

Two additional sets of samples were prepared by NREL using the ultra-high deposition HWCVD conditions: one set was prepared at different thicknesses and the second with different substrate temperatures. All were made at a deposition rate of 11 nm/s and with 2 filaments. Figure 11 shows the SAXS data from the thickness series and Figure 12 from the temperature series. Both plots show systematic behavior: a) the shape of the SAXS data changes to one of increasingly larger scattering features as the thickness increases by about a factor of 10, from about 4.8 nm to about 9.8 nm average dimension; b) the integrated SAXS drops by a factor of 10 as the temperature during deposition increases from $275^{\circ}C$ to $412^{\circ}C$, without much change in the shape of the SAXS curve. Some tilting experiments (Fig. 11) with these samples show highly oriented microstructure (the integrated SAXS drops by up to a factor of 5 upon tilting the sample by 35 degrees).
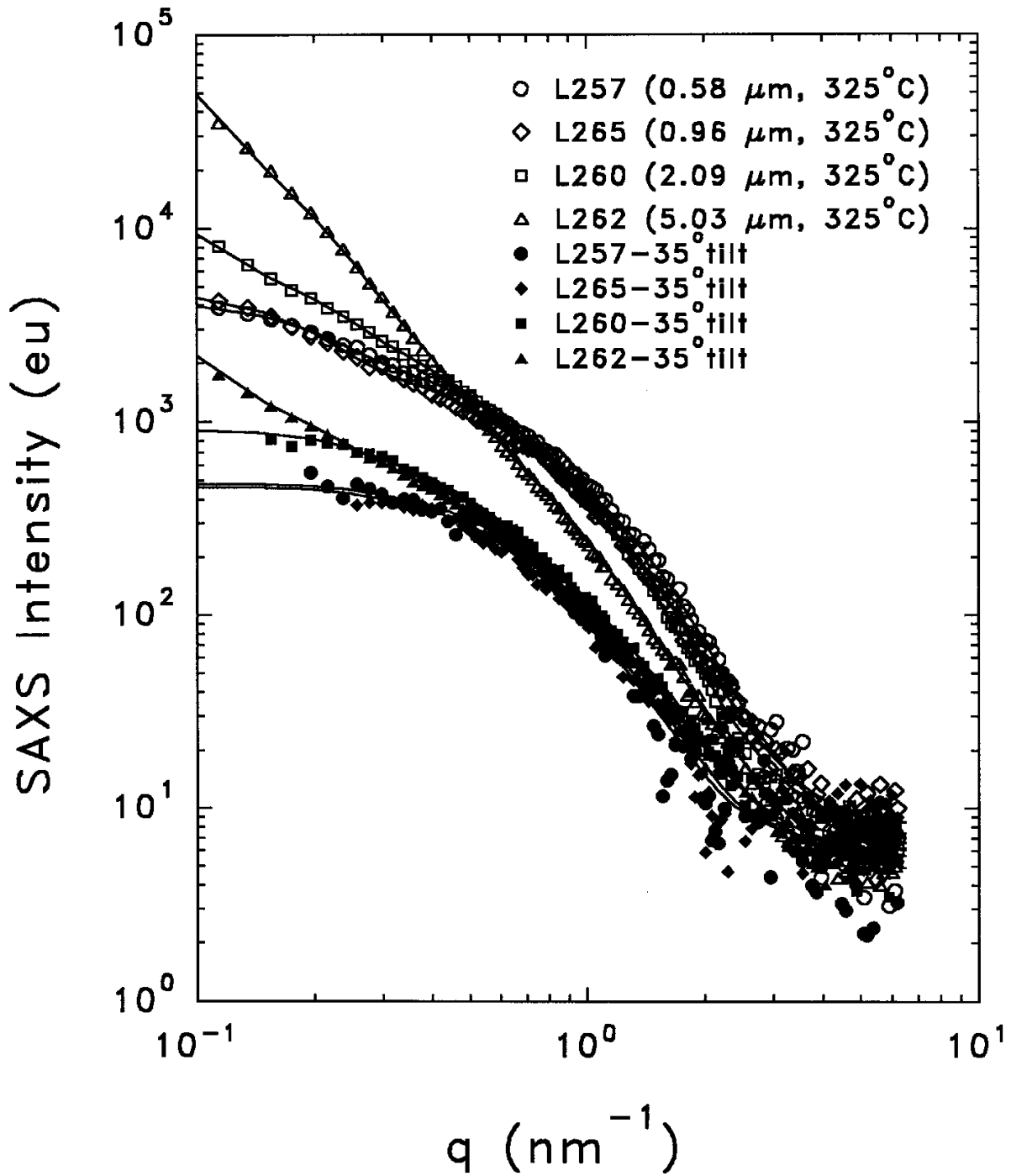
15

Fig.11. SAXS data from thickness series of ultra-high deposition rate HWCVD a-Si:H films as well as tilting data for the same films. All films deposited at 11 nm/s.
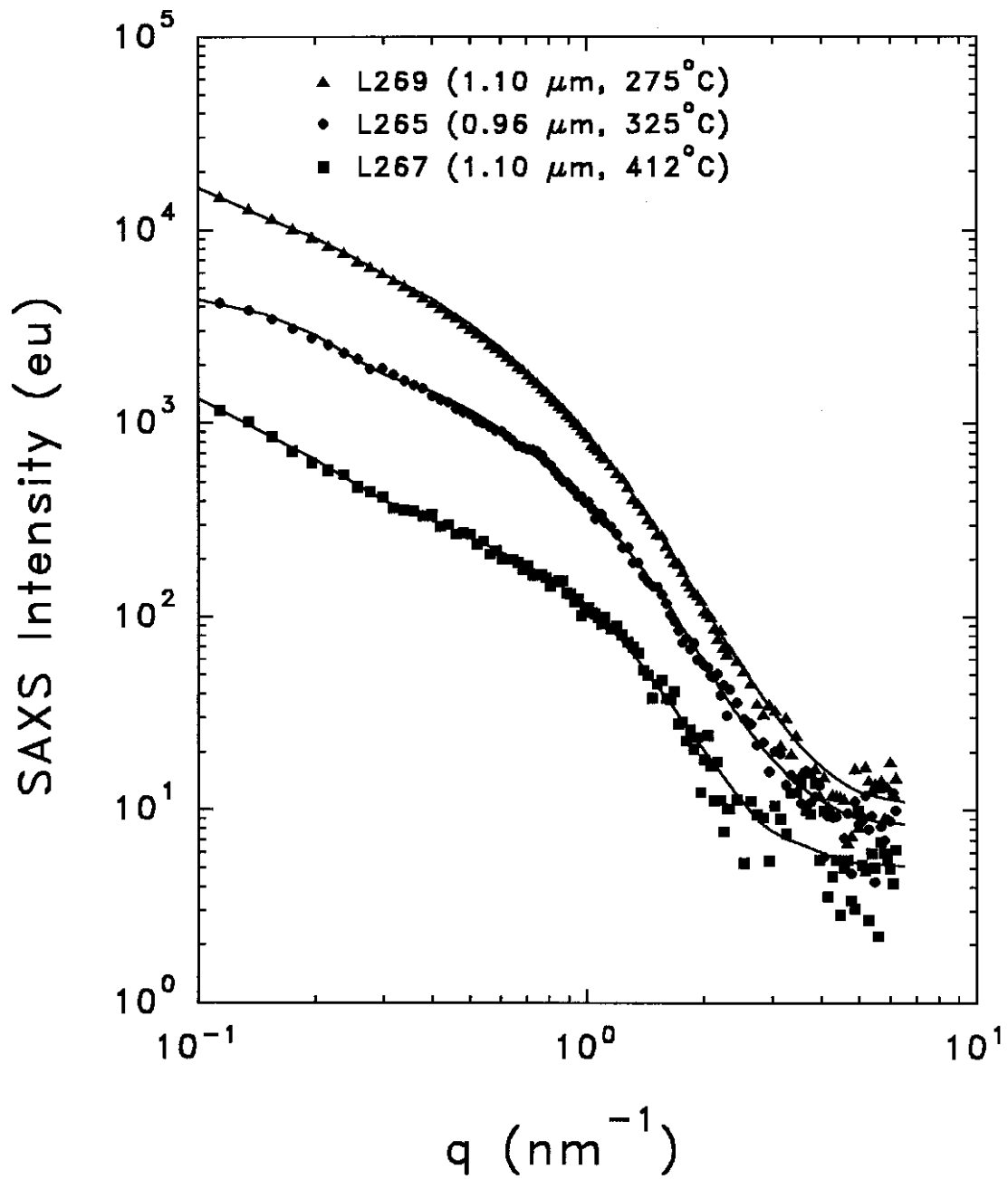
Fig. 12. SAXS data from temperature series of ultra-high deposition rate HWCVD a-Si:H. All films deposited at 11 nm/s.

3.4 "On-the-Edge" a-Si:H

Early Crystallization Study

PECVD films prepared by USSC under different H dilution conditions have been examined by IR, XRD, and H evolution. The high-H-dilution material is deemed "on-the-edge" material because of its observed tendency to be near the boundary between amorphous and microcrystalline states [27]. Figure 13 shows XRD data that yields no evidence of microcrystallites in the as-grown state. Upon annealing, a low temperature H-evolution peak appears, and film crystallization is observed at temperatures as low as 500°C, which is far below that observed for a-Si:H films grown without H dilution. Although not detected directly by XRD in the as-grown state, very small crystallites are postulated that catalyze the low-temperature crystallization of the films upon annealing [27]. The large spatial inhomogeneity in the H bonding associated with the very small
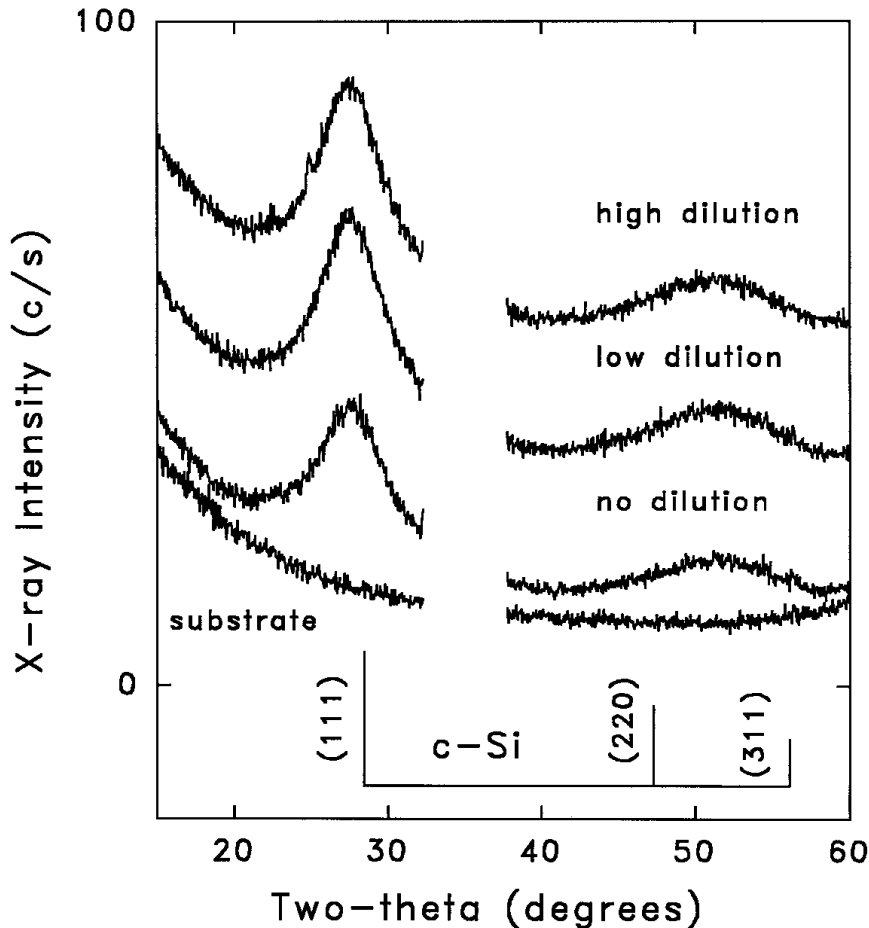

Fig. 13. XRD patterns from USSC a-Si:H films made at different hydrogen dilutions. Stick diagram for crystalline Si shown.

crystallites is suggested to be one of the reasons for the reduced Staebler-Wronski effect observed in solar cells utilizing the "on-the-edge" material [27].

Electronic States/XRD Study

Thin film n-i-p solar cells were prepared by USSC using decomposition of disilane-hydrogen mixtures by plasma-enhanced chemical vapor deposition. By increasing either the H dilution ratio or the thickness, the i-layer structure showed a transition from amorphous to microcrystalline silicon characterized by x-ray diffraction [28]. The electronic states of the i-layer were also examined by photoluminescence (PL) spectroscopy [28], which showed that: (a) below the onset of microcrystallinity, a blueshift of the 1.4 eV PL peak energy along with a decrease of the band width occur as the structural order is improved; (b) above the onset of microcrystallinity, the PL efficiency decreases by a factor of 4-5 and the PL peak energy is redshifted toward 1.2 eV as the μc-Si volume fraction is increased. In addition, the solar cell open circuit voltage shows first an increase and then a decrease, correlating with the PL peak energy position. We conclude that the PL spectroscopy is a sensitive tool for characterizing the gradual amorphous-to-microcrystalline structural transition in thin film solar cells [28].

3.5 ASAXS Experiments and Analyses

From extended anomalous-SAXS (ASAXS) measurements at numerous x-ray energies, structural and physical properties such as non-uniform Ge-concentrations and – in combination with flotation density results – the densities of Ge-enriched regions in amorphous a-$Si_{1-x}Ge_x$:H alloys were deduced based on a two-phase model [29]. Depending on the preparation technique (with and without H dilution of the source gases), a dense phase with volume fractions of about 90% and with Ge-enrichments only slightly higher with respect to the entire alloy were observed. These denser regions with average sizes between 10 and 23 nm can be interpreted as a phase containing slightly enhanced numbers of homopolar Ge-bonds, surrounded by a small volume fraction phase of low density, H-rich regions containing much less Ge (sometimes none) with averages sizes from 0.6 to 1.6 nm [29].

3.6 BP-Solarex SAXS/MRO Study

Four samples, one a-Si:H and three a-$Si_{1-x}Ge_x$:H alloys, were supplied by BP-Solarex (via Gautam Ganguly). SAXS and XRD measurements were supplemented by IR (for H content) and

EPMA (for x) done at NREL. Figure 14 shows the SAXS data and fits for the 4 samples. There is a systematic increase as Ge is added, consistent with our typical observations. This trend is also shown in Figure 15 where the integrated SAXS, Q_N, due to nanostructural features, is compared with results from many other Si-Ge alloys. A line has been added to show the trend in the BP-Solarex samples. The a-Si:H sample is somewhat higher than the usual value of $\sim 2 \times 10^{22}$ eu/cm^3 for device-quality material, but the three Ge alloys lie at the low side of the data shown (except for the two USSC microwave alloys which were prepared under high bias).
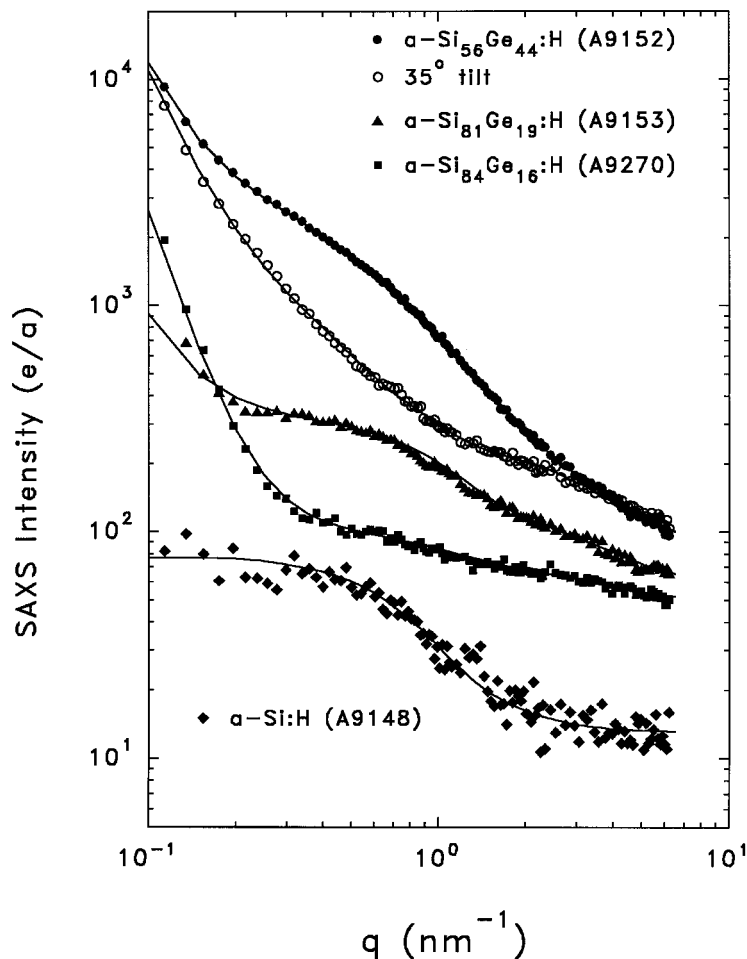

Fig. 14. SAXS data for a-Si$_{1-x}$Ge$_x$:H alloy films from BP-Solarex. Solid lines are fits based on distribution of spherical objects. Tilting data included for one sample.
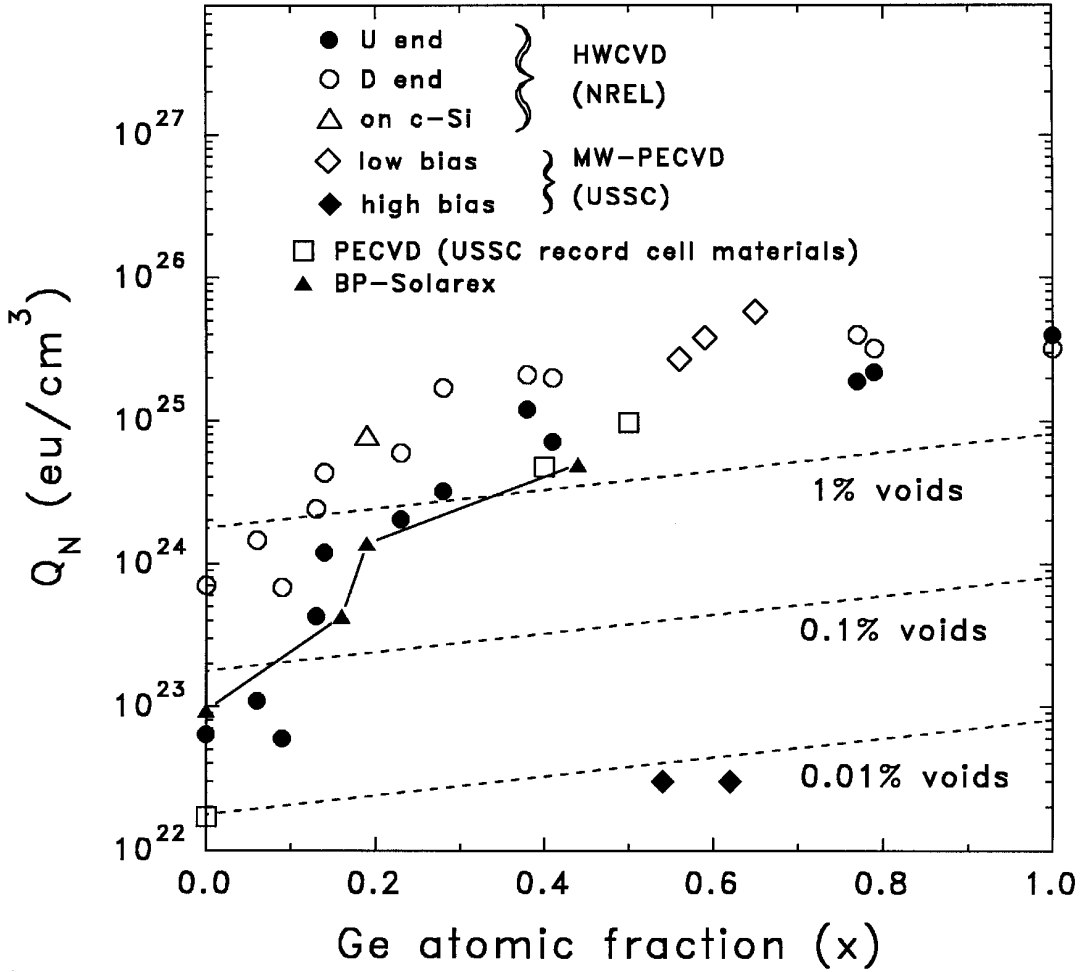
Fig. 15. Survey of integrated SAXS results for a-Si$_{1-x}$Ge$_x$:H alloys prepared by different groups and methods, highlighting the BP-Solarex results.

Table IV summarizes the quantitative information from these samples. The hydrogen content was based on the 640 cm^{-1} IR line. The SAXS data were fitted with a sum of the 3 contributions discussed in reference 1. The large increase in diffuse scattering, I$_D$, is consistent with the atomic-scale scattering from Si-Ge-H alloys with increasing Ge content. <D> represents the average diameter of spherical objects used to fit the data. These may be nanovoids or Ge composition fluctuations as demonstrated in our ASAXS studies [29,30]. Figure 14 includes SAXS data from a tilting experiment and this clearly demonstrates that the scattering features are non-spherical and oriented with longer axes parallel to the growth direction, a typical observation for Si-Ge alloys [1]. The flotation density of the a-Si:H sample was measured and found to be 2.18 g/cm^3, which is consistent with a 15at.% H content and a small void fraction.

Table IV. Quantitative SAXS and IR results from BP-Solarex films.

Sample	Thickness (μm-via x-ray)	x	$[H]_{IR}$ (at.%)	Q_N (eu/cm^3)	A (eu/nm^3)	I_D (e/a)	$<D>$ (nm)
A9148	2.08	0	15.1	0.09E24	0	13	3.2
A9270	2.56	0.16	14.1	0.43E24	0.4	50	0.6
A9153	1.80	0.19	12.1	1.38E24	0.6	60	1.4
A9152	2.10	0.44	13.0	4.92E24	9.2	87	2.1

(eu = electron units = electrons/atom = e/a)

The same Solarex samples that were used for the IR measurements (on c-Si substrates) were examined by x-ray diffraction to look at the medium-range order (MRO). This is our first study of MRO with a-SiGe:H alloys. Since the c-Si substrates used had the (111) orientation (previous work utilized (100) orientation [4]) , there was a strong interference of the (111) peak with the first scattering peak (FSP) of the a-SiGe:H. This problem has been minimized by using an asymmetric x-ray diffraction mode to collect the data. The sample is kept at a fixed angle of six degrees relative to the incident beam and the 2-theta scattering angle is scanned. Figure 16 shows data from the 4 samples and the substrate. There is only a small residual contribution from the c-Si (111) peak. The intensities have been corrected with ratios of the thicknesses relative to that of the a-Si:H sample (2.08 μm) One can see the systematic increase in the scattered intensity with x (the higher-Z Ge atoms scatter x-rays more strongly) and even slight shifts downward in peak positions as the average interatomic distances decrease (the dashed lines are included to help see these shifts). Figure 17 shows the results of the analysis of the width W of the first sharp diffraction peak [4] versus Ge content and compares them to the previous ranges of W for a-Si:H materials made by other groups [4]. The MRO seems to be not quite as optimized as in the USSC high-dilution material or the HWCVD high-substrate-temperature material. Figure 17 includes a very recent sample provided by BP-Solarex (#A42-1) and a reduced W is found suggesting slightly improved MRO in this newer sample.

3.7 High-Pressure Study

At the request of the UCLA group, two SAXS samples were supplied for a high pressure experiment. These were HWCVD a-Si:H films on 10 micron Al foil, folded into 8 layers:
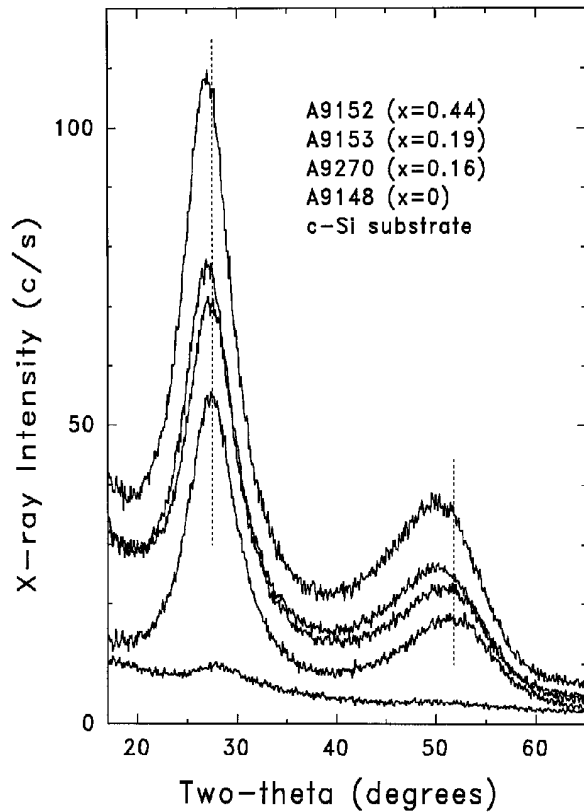
Fig. 16. XRD patterns from BP-Solarex
a-Si$_{1-x}$Ge$_x$:H films on (111) c-Si

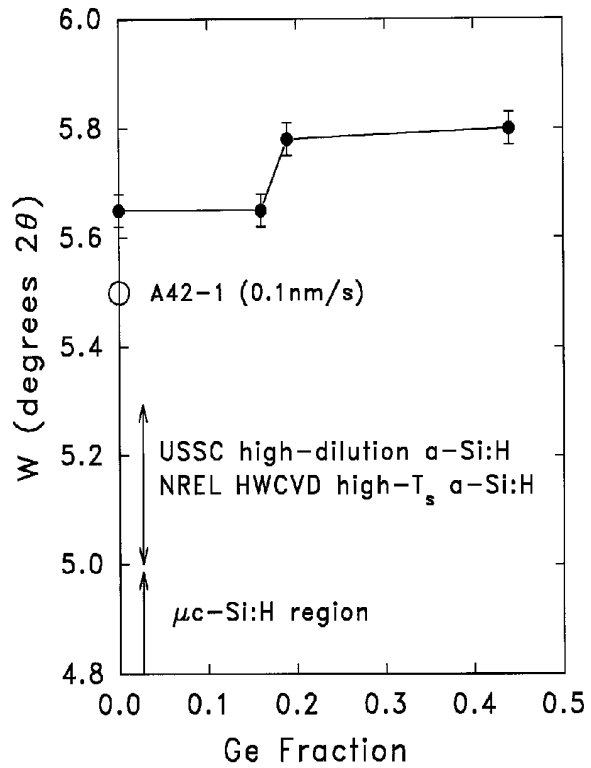Fig. 17. XRD linewidths of BP-Solarex
a-Si$_{1-x}$Ge$_x$:H films on (111) c-Si

T840 - low substrate temperature, relatively high void fraction (about 2 vol.%)

T905 - high substrate temperature, very low void fraction (about 0.02 vol.%)

A SAXS-reference Al-substrate foil was included in the high pressure treatment of the above samples. Figure 18 is a plot of the SAXS data comparing the intensities before and after the high pressure treatment (subjected to 3 kbar and released, repeated four times). The lower plot shows the ratios of the after/before intensities. It appears that there is no detectable effect. Quantitatively, the average ratio for T840 (the one with a high void density) is 1.005. The average for T905 is 0.939 but this includes many data points at high q which have large error bars due to the very weak signal. Averaging the first 45 points (q < 1.0 nm-1), then the average is 0.983. Since both of these samples show a significant tilting effect, such small changes (difference from unity) are readily explained by not having the sample in exactly the same position in the SAXS system before and after the treatment. Thus, there appears to be no evidence for a residual microvoid collapse after pressure treatment at 3 kbar. The UCLA group had postulated such a collapse to explain some irreversible electronic behavior after such a treatment.
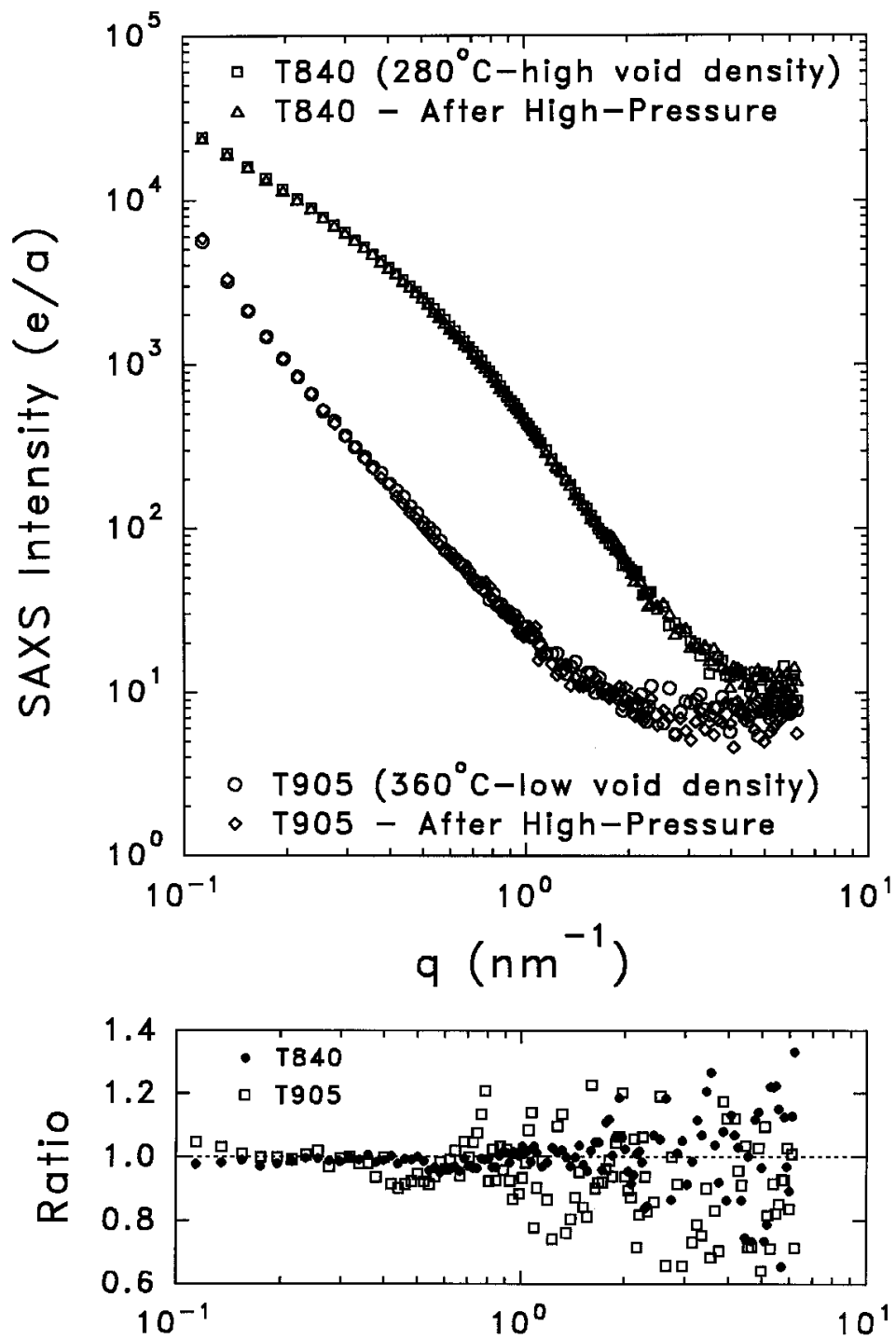
Fig. 18. (upper) SAXS data before and after a 3 kbar high-pressure treatment on two HWCVD films with different void content. (lower) Ratios of after/before intensities.

3.8 "Polymorphous" Si:H

SAXS measurements have been completed for a series of a-Si:H samples that are designated as "polymorphous" (pm) to describe a new type of a-Si:H by P. Cabarrocas of the Ecole Polytechnique [31]. This material apparently contains significant amounts of crystalline clusters imbedded in the amorphous matrix and evidence is found for improved transport properties and enhanced stability [31-33]. Figure 19 shows the SAXS data and fits. The SAXS is mostly composed of a Porod term (A/q^3) and a diffuse term (I_D =constant vs q) for all samples. The Porod

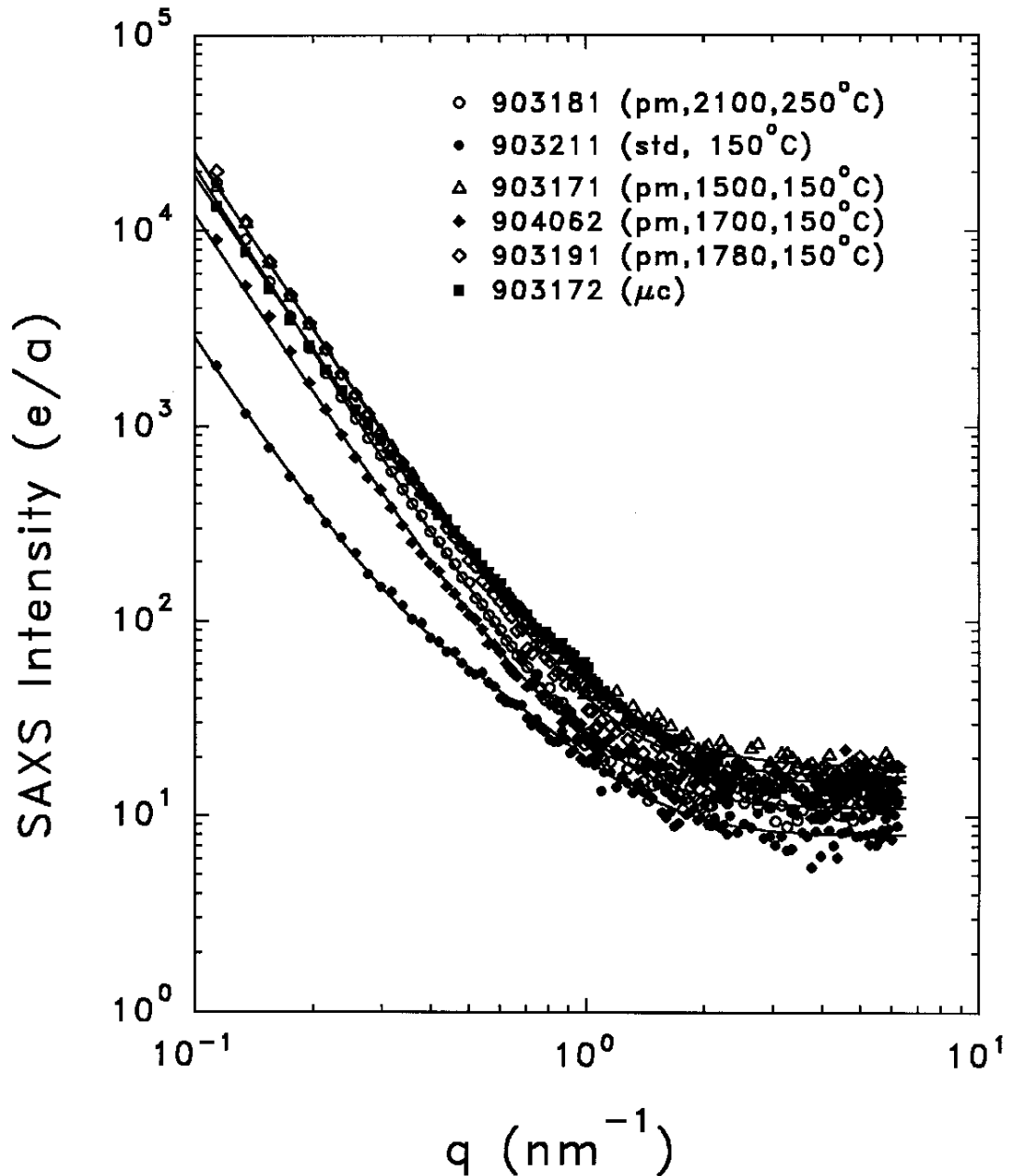

Fig. 19. SAXS data from Ecole-Polytechnique polymorphous (pm)-Si:H, standard a-Si:H, and partially microcystalline (μc)–Si:H.

scattering is due to some larger-scale structural features at least 20 nm in size. This could be surface-roughness related since the SAXS from the two c-Si substrate samples measured so far have much reduced A/q^3 terms. Differences in I_D (see range of intensity levels at high q) are likely related to differences in bonded H content. The SAXS due to any nanostructural features (< 10 nm) is extremely weak. Only samples 903171, 903211, and 903172 show a component (Q_N) slightly larger than the detection limit of $Q_N = \sim 2 \times 10^{22}$ eu/cm^3 (corresponding to 0.01 vol.% voids). Thus, it is very interesting that there is little or no scattering from the "polymorphous" nature of these films! This may be due to a very small electron density contrast between the incorporated nanocrystals that are seen by TEM [31,32] and the amorphous matrix, and/or due to a very small volume fraction of such nanocrystals (however, Cabarrocas has pointed out that he expects the films to have large volume fractions). We measured XRD on all the polymorphous samples and did not detect any evidence of crystalline Si (111), (220), or (311) peaks. These peaks were detected in 903172 (the sample known to be partially μc) but it was still mostly amorphous.
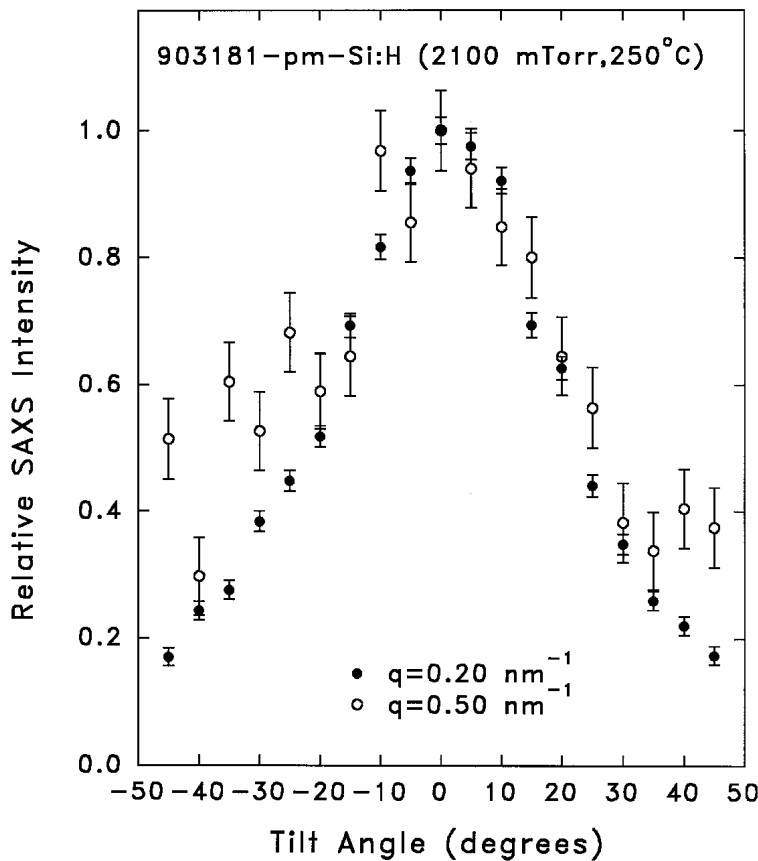
Detailed tilting experiments were done on one of the polymorphous samples that was deposited on both Al-foil and thin c-Si suitable for SAXS. Figure 20 shows a strong tilt effect for the film deposited on Al-foil. The intensity was measured at two values of q, one where the SAXS intensity is quite high (q=0.2 nm^{-1}) and one where to intensity is quite low (q=0.5 nm^{-1}). The symmetric drop of intensity by about a factor of 5 at ±45° is consistent with elongated scattering objects aligned with the growth direction (i.e., columnar-like features). This effect makes it difficult to attribute the

Fig. 20. Tilting data from a polymorphous Si:H film on Al-foil.

small q scattering to surface roughness. Based on ellipsoidal objects, the drop of a factor of 5 can be explained by objects with major-to-minor axis ratios of about 9 that are aligned with the long axis along the growth direction. This would correspond to rather large objects since the scattering is at relatively low q (>10 nm for the minor axis size!). These objects cannot be the nanocrystals expected in the polymorphous material since the TEM studies indicate 2 to 4 nm sizes [31,32]. Surprisingly, the results from films on the c-Si substrates are quite different as illustrated in Fig. 21. The film on Si yields a much lower Porod scattering and there is no detectable tilting effect. This provides strong evidence of a significant substrate effect on the growth and microstructure of the polymorphous material.
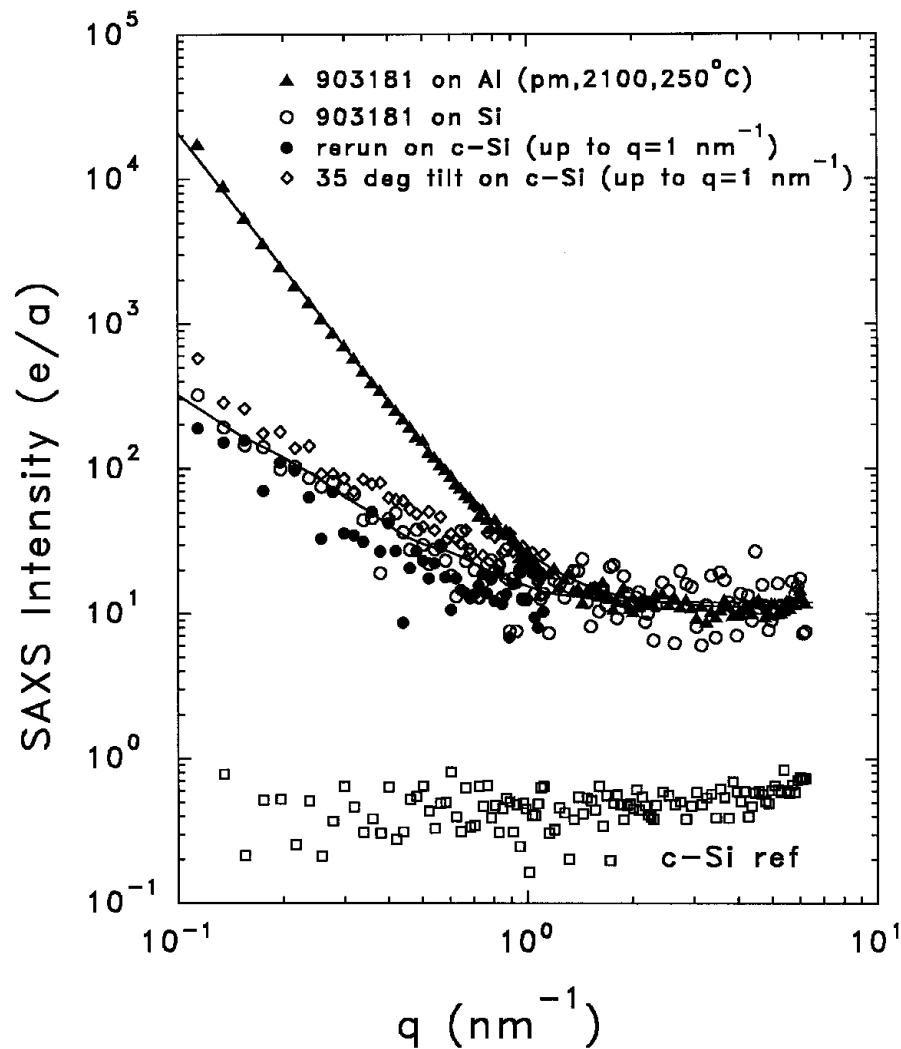

Fig. 21. SAXS data from polymorphous (pm)-Si:H co-deposited on Al-foil and on c-Si. Tilting at 35 degrees cause little change for the film on c-Si.

We also provide results on the density of the polymorphous Si:H. Table V lists the values obtained by the flotation density method from the same samples used to obtain the SAXS data in Fig. 19. The polymorphous samples are only slightly less dense than the standard a-Si:H and this is likely due to a higher H content consistent with the larger diffuse scattering levels seen for the polymorphous films in Fig. 19. Note the increased density due to the higher substrate temperature used for sample 903181. The observed density deficit relative to c-Si (2.33 g/cm^3) is typical of a-Si:H with 8-15 at.% bonded H [34].

Table V. Flotation densities of polymorphous, standard, and partially microcrystalline Si:H.

Sample	Structure (prep)	Density (g/cm^3)
903211	Standard, fully amorphous a-Si:H (Ts=150°C)	2.201
903172	Microcrystalline Si:H	2.177
903172	Polymorphous Si:H (1600 mTorr, Ts=150°C)	2.180
904062	Polymorphous Si:H (1700 mTorr, Ts=150°C)	2.180
903191	Polymorphous Si:H (1800 mTorr, Ts=150°C)	2.181
903181	Polymorphous Si:H (2100 mTorr, Ts=250°C)	2.228

3.9 Microcrystalline Si:H

Due to increased interest in microcrystalline Si for possible solar cell applications, three sets of such material from different groups were examined by SAXS, XRD, and flotation density.

HMI Material

SAXS and density measurements have been completed on four μc-Si:H samples sent by M. Birkholz of the Hahn-Meitner-Institut (HMI). The samples were deposited by microwave PECVD at 325°C under a series of applied biases from 0 to +45 V. Figure 22 shows that the SAXS signals are quite strong compared to device-quality PECVD a-Si:H and there are not dramatic differences in the 4 samples prepared at different biases. A fit of a spherical particle distribution is shown in Fig. 23 for one of the samples where the inset gives the distribution and average diameter. Table VI gives the quantitative results for the 4 samples. The integrated intensity from the nanostructural features, Q_N, can be used to estimate a volume fraction of voids, assuming this is the origin of the SAXS. These values are listed as f in the table. There appear to be systematic trends in Porod slope, A (larger-scale structure contributions affecting slope at low q), diffuse scattering, I_D (typically this

increases with bonded H content), and <D>. These effects can be seen in Fig. 22 by comparing just the NTi-086 and NTi-089 data (the larger sizes for NTi-089 are evident by the shift of the curve to lower q and the larger I_D is seen at the largest q).

Table VI. Quantitative results from HMI microcrystalline-Si:H films.

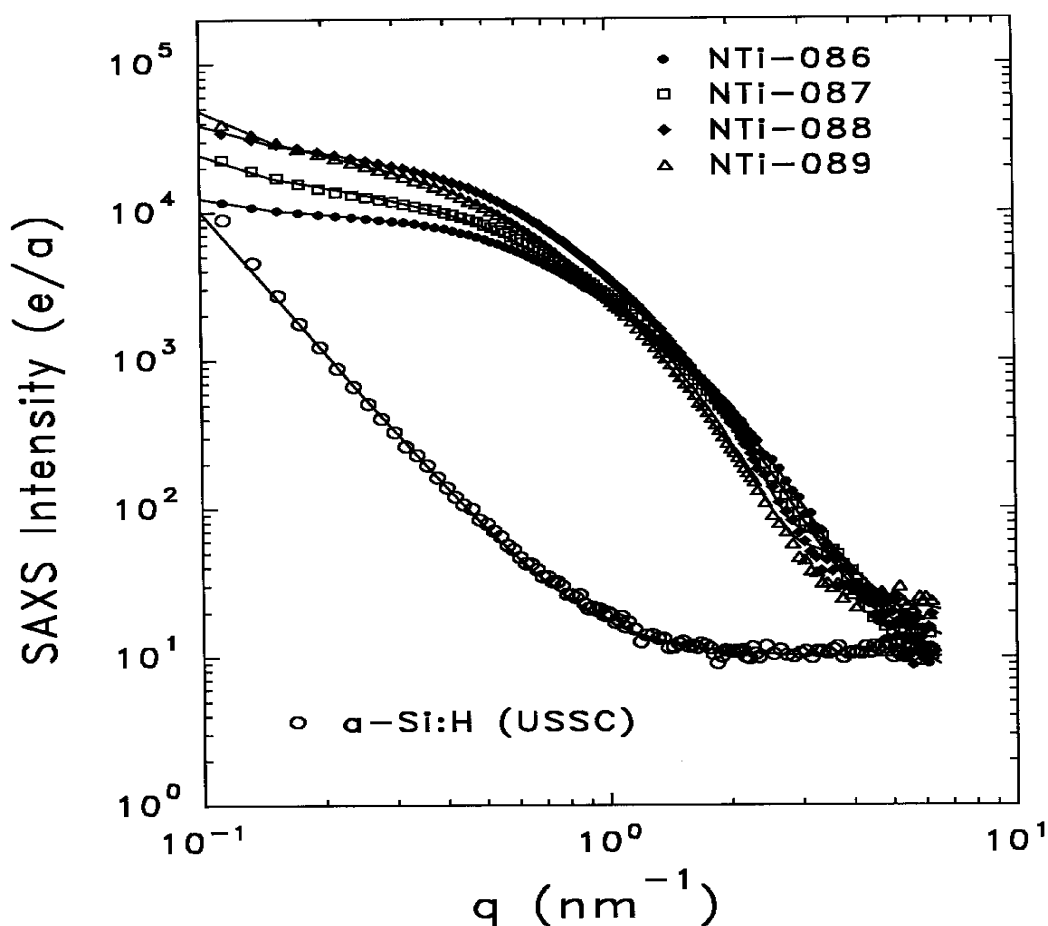| Sample	Bias (V)	thickness(μm)	Q_N(eu/cm3)	A(eu/nm^3)	I_D(eu)	<D>(nm)	ρ_{flot}(g/cm^3)	f(%)
NTi-086	0	2.2	1.21E25	3	4	3.7	2.18	6.7
NTi-087	+15	1.5	1.30E25	10	5	4.3	2.23	7.2
NTi-088	+30	1.3	1.83E25	14	9	5.1	2.18	10.6
NTi-089	+45	1.4	1.37E25	25	17	5.7	2.18	7.7

(eu = electron units = electrons/atom = e/a)

Fig.22. SAXS data from microcrystalline Si:H preprared at the HMI by microwave-PECVD under different substrate biases. PECVD a-Si:H made at USSC shown for comparison.
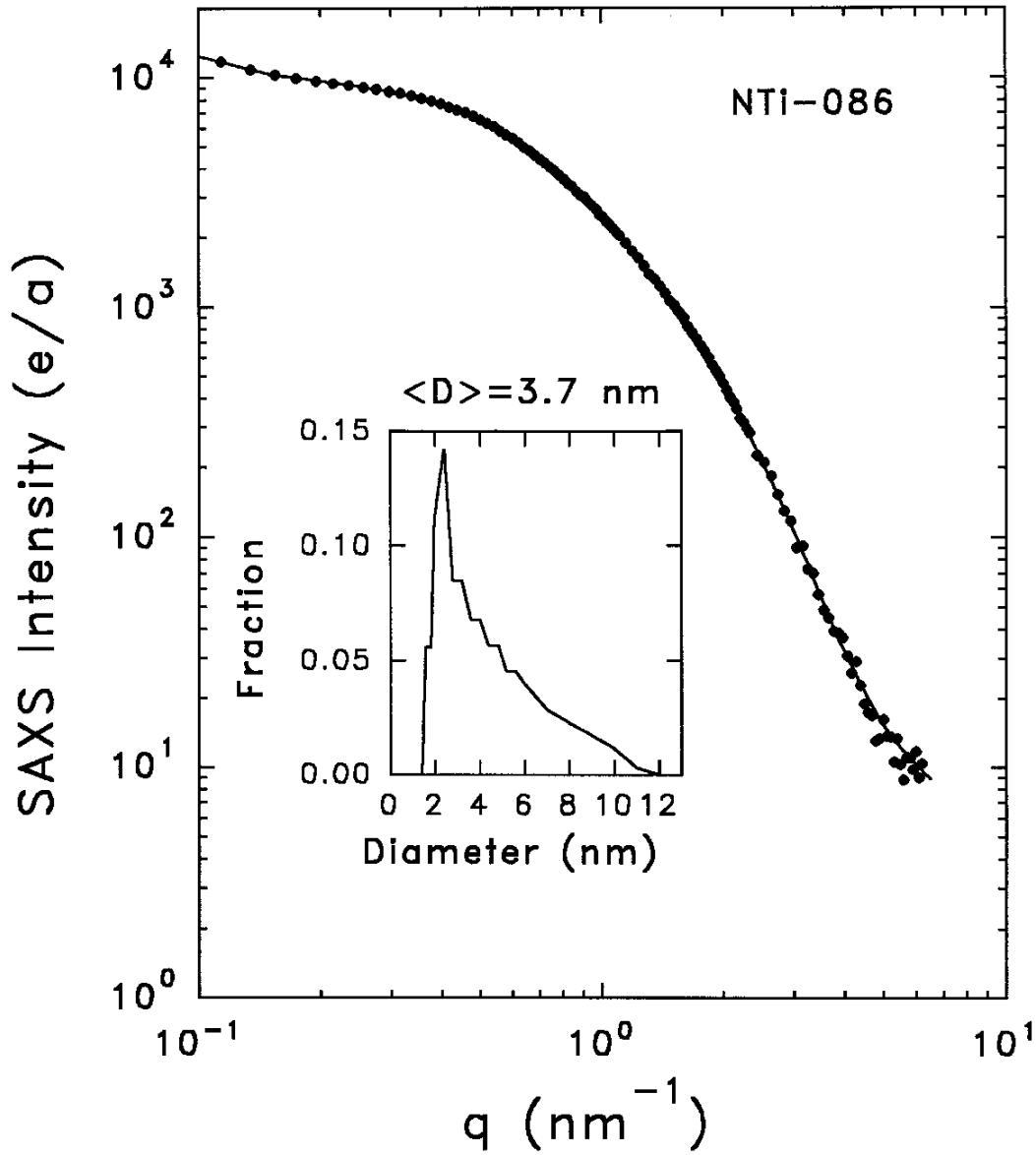
Fig. 23. Example of fit to the SAXS data from one of the HMI microcrystalline samples. Inset
shows distribution of spheres used in the fit and the average diameter.

ECD Gas Jet Material

Four samples of μc-Si:H prepared by the gas-jet technique developed at ECD [35] were
examined by SAXS. The silane flow was increased from 15 to 45 sccm for the series of samples
and the integrated SAXS was found to decrease systematically from a high value corresponding to

about 11% voids to a value for about 1.5% voids. This is consistent with an expected trend of decreasing amount of microcrystalline material with increasing gas flow [35]. This was confirmed by XRD. The scattering features are only about 2 nm in diameter and show a relatively weak tilting effect. Table VII provides the quantitative SAXS results. Note that the integrated SAXS from the lowest flow sample is comparable to the large values from the HMI µc-Si:H listed in Table VI.
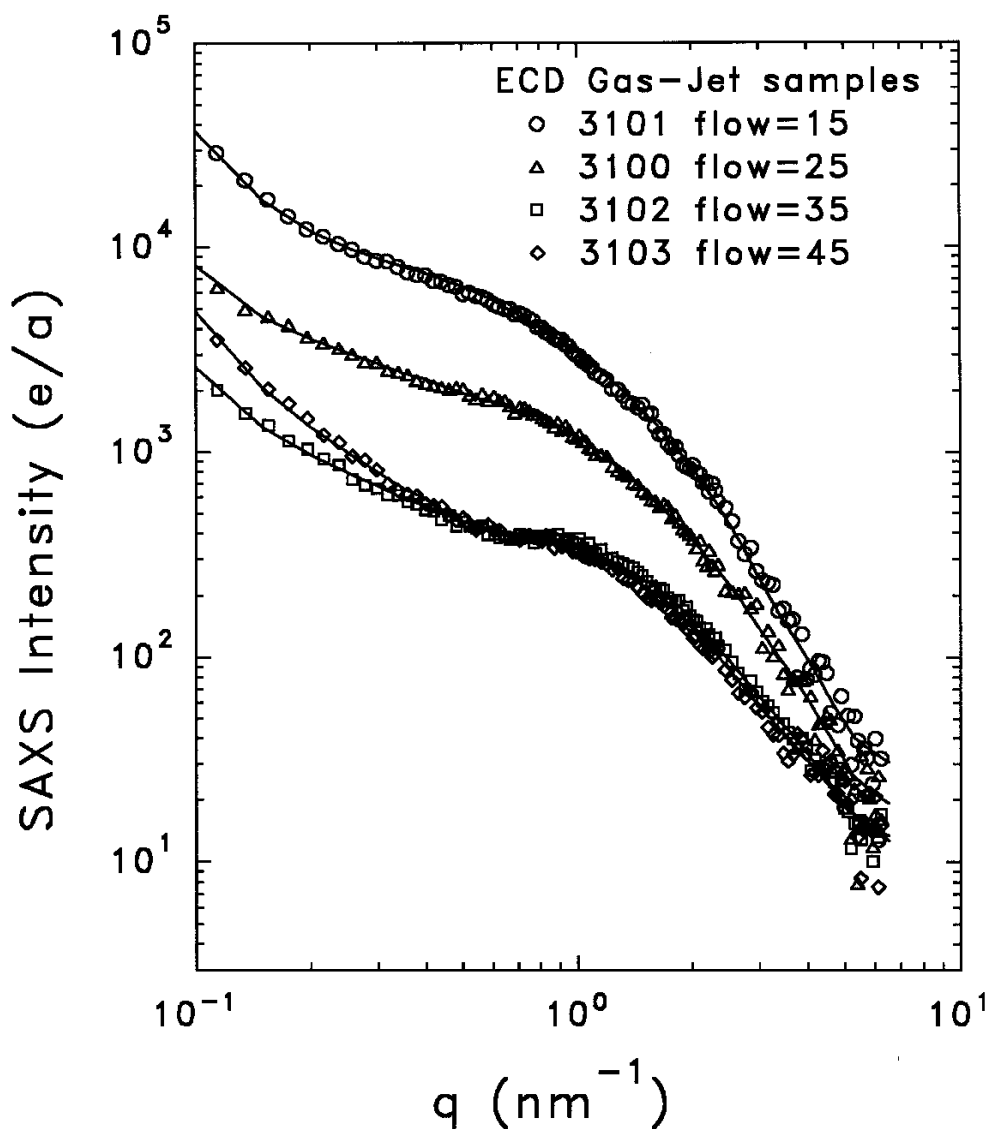

Fig. 24. SAXS data from ECD gas-jet microcrystalline films made under different gas flows.

Also, note that the thicknesses of the gas-jet films are quite small and this causes the data to be somewhat noisier in Fig. 24 compared to Figs. 22 and 23.

Table VII. Quantitative SAXS results from ECD gas-jet µc-Si:H.

Sample	flow	Thickness (µm)	Q_T(eu/cm^3)	Q_N(eu/cm^3)	A(eu/nm^3)	I_D(eu)	<D>(nm)
GJ3101	15	0.21	17.3E24	16.4E24	28	10	2.8
GJ3100	25	0.35	7.20E24	7.04E24	5.0	11	2.3
GJ3102	35	0.63	2.60E24	2.54E24	1.8	8	1.8
GJ3103	45	0.70	2.44E24	2.31E24	4.0	10	1.9

(eu = electron units = electrons/atom = e/a)

IPE Material

Four films of µc-Si:H prepared by the HWCVD method at the Institute of Physical Electronics (IPE) of the University of Stuttgart have been examined by SAXS. Quantitative results are listed in Table VIII. This series was made as a function of deposition pressure and yielded a minimum in the integrated SAXS at the intermediate value of 40 mTorr. The corresponding void volume fractions range from 11 to 6 %, again very high and apparently typical of microcrystalline material (compare with Tables VI and VII). The sizes of the scattering features range from 6 to 9 nm and clear, but relatively weak, tilting effects are observed. X-ray diffraction (XRD) patterns were also measured from the same films used for the SAXS and the preferred orientation (PO) is included in Table VIII.

Table VIII. Quantitative SAXS results from IPE HWCVD µc-Si:H

Sample	Pressure(mTorr)	t (µm)	Q_N (eu/cm^3)	A (eu/nm^3)	I_D (eu)	<D> (nm)	XRD (PO)
M002162	400	2.1	1.67E25	60	9	9.4	(220)
M002171	100	2.2	1.23E25	30	7	6.8	(111)
M002182	40	2.4	1.00E25	30	4	5.7	(111)
M002172	10	2.5	1.36E25	60	5	5.7	(220)

M002162 tilt ratio $Q(0^o)/Q(35^o) = 2.3$
M002182 tilt ratio $Q(0^o)/Q(35^o) = 2.3$

The I_D parameter is related to the amount of H dispersed on the atomic scale in the samples. The values in the table are consistent with rather low H contents typically seen in HWCVD samples grown at the typical elevated temperatures of about 360° or higher (< 7 at.%). There also seems to

be a trend of decreasing I_D with increasing sample number as listed in the table. However, these values are quite uncertain since it is based on the data at high q where there is more scatter in the data.

We have now accumulated considerable data for microcrystalline Si:H and the development of a model to account for the strong SAXS is in order.

4. REFERENCES

1. D.L. Williamson, Mater. Res. Soc. Symp. Proc. **377**, 251 (1995) and references therein.

2. S. Guha, J. Yang, S.J. Jones, Yan Chen, and D.L. Williamson, Appl. Phys. Lett. **61**, 1444 (1992).

3. S. Guha, J. Yang, D.L. Williamson, Y. Lubianiker, J.D. Cohen, and A.H. Mahan, Appl. Phys. Lett. **74**, 1860 (1999).

4. D.L. Williamson, Mater. Res. Soc. Symp. Proc. **557**, 251 (1999) and references therein.

5. A.J. Leadbetter, A.A.M. Rashid, R.M. Richardson, A.F. Wright, and J.C. Knights, Solid State Commun. **33**, 973 (1980).

6. T.A. Postol, C.M. Falco, R.T. Kampwirth, I.K. Schuller, and W.B. Yelon, Phys. Rev. Lett. **45**, 648 (1980).

7. A.J. Leadbetter, A.A.M. Rashid, N. Colenutt, A.F. Wright, and J.C. Knights, Solid State Commun. **38**, 957 (1981).

8. R. Bellissent, A. Chenevas-Paule, and M. Roth, J. Non-Cryst. Solids **59&60**, 229 (1983); Physica B **117&118**, 941 (1983).

9. A. Chenevas-Paule, R. Bellissent, M. Roth, and J.I. Pankove, J. Non-Cryst. Solids **77&78**, 373 (1985).

10. C.A. Guy, A.F. Wright, R.N. Sinclair, R.J. Stewart, and F. Jansen, J. Non-Cryst. Solids **196**, 260 (1996).

11. T.P. Russel, P. Lambooy, J.C. Barker, P. Gallagher, S.K. Satija, G.J. Kellogg, and A.M. Mayes, Macromolecules **28**, 787 (1995).

12. D.L. Ho, R.M. Briber, R.L. Jones, S.K. Kumar, and T.P. Russel, Macromolecules **31**, 9247 (1998).

13. L.A. Feigin and D.I. Svergun, *Structure Analysis by Small-Angle X-ray and Neutron Scattering* (Plenum, New York, 1987).

14. D.W.M. Marr, M. Wartenberg, K.B. Schwatz, M.M. Agamalian, and G.D. Wignall, Macromolecules **30**, 2120 (1997).

15. A. Menelle, J. Non-Cryst. Solids **97&98**, 337 (1987).

16. R. Bellissent, in *Amorphous Silicon and Related Materials*, ed. H. Fritzche (World Scientific, 1988) p.93.

17. J. Yang, A. Banerjee, and S. Guha, Appl. Phys. Lett. **70**, 2975 (1997).

18. Q. Wang, E. Iwaniczko, Y. Xu, B.P. Nelson, and A.H. Mahan, Mater. Res. Soc. Symp. Proc. **557**, 163 (1999).

19. C.J. Glinka, J.G. Barker, B. Hammouda, S. Krueger, J.J. Moyer, and W.J. Orts, J. Appl. Cryst. **31**, 430 (1998).

20. B.P. Nelson, Y. Xu, A.H. Mahan, D.L. Williamson, and R.S. Crandall, Mater. Res. Soc. Symp. Proc. (2000, in press).

21. H. Fritzsche, Mater. Res. Soc. Symp. Proc. **467**, 19 (1997), and references therein.

22. H. Chatam and P.K. Bhat, Mat. Res. Soc. Symp. Proc. **149**, 447 (1989).

23. A. Shah, J. Dutta, N. Wyrsch, K. Prasad, H. Curtins, F. Finger, A. Howling, and Ch. Hollenstein, Mat. Res. Soc. Symp. Proc. **258**, 15 (1992).

24. S.J. Jones, X. Deng, T. Liu, and M. Izu, Mat. Res. Soc. Symp. Proc. **507**, 113 (1998).

25. J. Yang, S. Sugiyama, S. Guha, Mat. Res. Soc. Symp. Proc. **507**, 157 (1998).

26. B.P. Nelson, Y. Xu, A.H. Mahan, D.L. Williamson, and R.S. Crandall, Mat. Res. Soc. Symp. Proc. (2000, in press).

27. A.H. Mahan, J. Yang, S. Guha, and D.L. Williamson, Phys. Rev. **B61**, 1677 (2000).

28. G. Yue, D. Han, D.L. Williamson, J. Yang, K. Lord, and S. Guha, submitted to APL (2000).

29. G. Goerigk and D.L. Williamson, submitted to JAP (2000).

30. G. Goerigk and D.L. Williamson, Solid State Commun. **108**, 419 (1998).

31. P. Roca i Cabarrocas, S. Hamma, S.N. Sharma, G. Viera, E. Bertran, and J. Costa, J. Non-Cryst. Solids **227-230**, 871 (1998).

32. J. Costa, P. Roura. P. Roca i Cabarrocas, G. Viera, and E. Bertan, Mat. Res. Soc. Symp. Proc. **507**, 499 (1998).

33. C. Longeaud, J.P. Kleider, M. Gauthier, R. Bruggemann, Y. Poissant, and P. Roca i Cabarrocas, Mat. Res. Soc. Symp. Proc. **557**, 501 (1999).

34. Y. Chen, Ph.D. Thesis, Colorado School of Mines (1994).

35. S.J. Jones, R. Crucet, X. Deng, J. Doehler, R. Kopf, A. Myatt, D.V. Tsu, and M. Izu, Mat. Res. Soc. Symp. Proc. **557**, 567 (1999).

REPORT DOCUMENTATION PAGE

1. AGENCY USE ONLY (Leave blank)	2. REPORT DATE October 2000	3. REPORT TYPE AND DATES COVERED Annual Technical Progress Report; 22 May 1999 – 21 August 2000

4. TITLE AND SUBTITLE
Nanostructure of a-Si:H and Related Alloys by Small-Angle Scattering of Neutrons and X-Rays; Annual Technical Progress Report; 22 May 1999 – 21 August 2000

5. FUNDING NUMBERS
C: XAK-8-17619-31
TA: PVP15001

6. AUTHOR(S)
D.L. Williamson

7. PERFORMING ORGANIZATION NAME(S) AND ADDRESS(ES)
Department of Physics
Colorado School of Mines
Golden, Colorado 80401

8. PERFORMING ORGANIZATION REPORT NUMBER

9. SPONSORING/MONITORING AGENCY NAME(S) AND ADDRESS(ES)
National Renewable Energy Laboratory
1617 Cole Blvd.
Golden, CO 80401-3393

10. SPONSORING/MONITORING AGENCY REPORT NUMBER

NREL/SR-520-29121

11. SUPPLEMENTARY NOTES

NREL Technical Monitor: B. von Roedern

12a. DISTRIBUTION/AVAILABILITY STATEMENT
National Technical Information Service
U.S. Department of Commerce
5285 Port Royal Road
Springfield, VA 22161

12b. DISTRIBUTION CODE

13. ABSTRACT *(Maximum 200 words).* This report describes work being performed to provide details of the microstructure in high-quality hydrogenated amorphous and microcrystalline silicon and related alloys on the nanometer size scale. The materials under study are being prepared by current state-of-the-art deposition methods, as well as by new and emerging deposition techniques. The purpose is to establish the role of nanostructural features in controlling the opto-electronic and photovoltaic properties. The approach centers around the use of the uncommon technique of small-angle scattering of both X-rays (SAXS) and neutrons (SANS). SAXS has already been established as highly sensitive to microvoids and columnar-like microstructure. A major goal of this research is to establish how sensitive SANS is to the hydrogen nanostructure. Conventional X-ray diffraction techniques are being used to examine medium-range order and microcrystallinity, particularly near the boundary between amorphous and microcrystalline material.

14. SUBJECT TERMS
photovoltaics; amorphous-silicon solar cell; thin-film materials; multijunction solar cells; opto-electronic properties; device performance; small-angle X-rays scattering (SAXS); small-angle neutrons scattering (SANS); Ge uniformity; nanostructure in a-SiGe:H; a-Si:H; plasma-enhanced chemical-vapor deposition (PECVD); Staebler-Wronski; hydrogenated and deuterated films; polycrystalline; microcrystalline

15. NUMBER OF PAGES

16. PRICE CODE

17. SECURITY CLASSIFICATION OF REPORT Unclassified	18. SECURITY CLASSIFICATION OF THIS PAGE Unclassified	19. SECURITY CLASSIFICATION OF ABSTRACT Unclassified	20. LIMITATION OF ABSTRACT UL